

This is an Open Access document downloaded from ORCA, Cardiff University's institutional repository: <https://orca.cardiff.ac.uk/id/eprint/177378/>

This is the author's version of a work that was submitted to / accepted for publication.

Citation for final published version:

Qu, Jiawei, Hou, Kai, Liu, Zeyu, Zhou, Yue , Zhu, Lewei, Dong, Xiaohong, Mu, Yunfei and Jia, Hongjie 2025. A hybrid time-and-event-driven strategy for integrated community energy system planning. Applied Energy 384 , 125274. 10.1016/j.apenergy.2025.125274

Publishers page: <http://dx.doi.org/10.1016/j.apenergy.2025.125274>

Please note:

Changes made as a result of publishing processes such as copy-editing, formatting and page numbers may not be reflected in this version. For the definitive version of this publication, please refer to the published source. You are advised to consult the publisher's version if you wish to cite this paper.

This version is being made available in accordance with publisher policies. See <http://orca.cf.ac.uk/policies.html> for usage policies. Copyright and moral rights for publications made available in ORCA are retained by the copyright holders.



A Hybrid Time-and-Event-Driven Strategy for Integrated Community Energy System Planning

Jiawei Qu^{a,b}, Kai Hou^{a,b*}, Zeyu Liu^{a,b*}, Yue Zhou^{a,c}, Lewei Zhu^d, Xiaohong Dong^e, Yunfei Mu^{a,b}, Hongjie Jia^{a,b}

^aKey Laboratory of Smart Grid of Ministry of Education, Tianjin University, Tianjin 30072, China

^bKey Laboratory of Smart Energy & Information Technology of Tianjin Municipality, Tianjin 30072, China

^cSchool of Engineering, Cardiff University, Cardiff CF24 3AA, U.K.

^dMaritime College, Tianjin University of Technology, Tianjin 300384, China

^eState Key Lab of Reliability and Intelligence of Electrical Equipment, Hebei University of Technology, Tianjin, 300130, China

E-mail: * khou@tju.edu.cn, tjulzy@tju.edu.cn

Author information:

Jiawei Qu was born in Heilongjiang, China. He is currently pursuing a Ph.D. degree at Tianjin University. His research interests are integrated energy system planning and reliability assessment.

Detailed address: Room A/303, Chengjiao Building, Tianjin University, Weijin Road No.92, Tianjin, 300072, China,

Email: jiawei_qu@tju.edu.cn, Tel: +86-18714325421

This work was financially funded by the National Natural Science Foundation of China program (No. 52077150) and the Enterprise Innovation and Development Joint Fund (No. U23B6006).

Highlights:

- 1) A hybrid time-and-event-driven strategy for multi-stage planning is proposed.
- 2) A framework for 8,760 normal and $N-k$ contingency scenarios analysis is developed.
- 3) A technology management method is proposed considering implicit costs.
- 4) A state-similarity method for analyzing massive scenarios is proposed.

A Hybrid Time and Event Driven Strategy for Integrated Community Energy Systems Planning

Jiawei Qu^{a,b}, Kai Hou^{a,b*}, Zeyu Liu^{a,b*}, Yue Zhou^{a,c}, Lewei Zhu^d, Xiaohong Dong^e, Yunfei Mu^{a,b}, Hongjie Jia^{a,b}

^aKey Laboratory of Smart Grid of Ministry of Education, Tianjin University, Tianjin 30072, China

^bKey Laboratory of Smart Energy & Information Technology of Tianjin Municipality, Tianjin 30072, China

^cSchool of Engineering, Cardiff University, Cardiff CF24 3AA, U.K.

^dMaritime College, Tianjin University of Technology, Tianjin 300384, China

^eState Key Lab of Reliability and Intelligence of Electrical Equipment, Hebei University of Technology, Tianjin, 300130, China

Abstract: Unpredictable events such as technological breakthroughs and energy policy shifts can cause significant errors in the forecast of the parameters like equipment performance and energy demands. Traditional single-stage and fixed multi-stage planning methods struggle with unpredictable events, severely impacting the accuracy of the planning of Integrated Community Energy Systems (ICES). As a solution, a Hybrid Time-and-Event-Driven Multi-Stage Planning (HTED-MSP) method is proposed for ICES. The HTED-MSP method determines the start time of each planning stage based on a combination of time and specific event. Specifically, the event-driven strategy mitigates unpredictable changes in load growth, energy prices, and technological advancements on costs, with trigger conditions determined by marginal cost analysis. Meanwhile, the time-driven strategy enhances long-term reliability of ICES. Considering the significant impact of renewable energy variability and equipment failures on reliability, the HTED-MSP method quantifies these factors using 8,760-hour normal and $N-k$ contingency scenarios. A State Similarity (SS) method is then proposed to address the computational burden of massive scenarios by simplifying the optimization process into an equation-solving approach. The case study demonstrates that HTED-MSP significantly reduces additional costs caused by unpredictable events. The computational efficiency of the SS method is more than ten times greater than the existing two-stage algorithms.

Keywords: Integrated Community Energy System; Multi-Stage Planning; Hybrid Time-and-Event-Driven; State Similarity; Reliability.

Nomenclature

Abbreviation

ICES	integrated community energy system	EB	electric boiler
MILP	mixed integer linear programming	PV	photovoltaics array
SSP	single stage planning	PT	photothermal collector
MSP	multi-stage planning	PH	photocatalytic reactor
HTED	hybrid time and event driven	SSS	solar spectrum splitting unit
RTR	replacement threshold rate	SOFC	solid oxide fuel cell
BD	benders decomposition	EL	electrolyser
SS	state similarity analysis method	WT	wind turbine
SS-Set	similar states set	P2G	power to gas system
POB	positions of the optimal bases	CC	carbon capture system
CHP	combined heat and power unit	P2GCC	power to gas and carbon capture system
ASHP	air source heat pump	ES	electricity storage
GHP	ground source heat pump	TS	thermal storage
GT	gas turbine	HS	hydrogen storage

Indices and Sets

p / \mathcal{P}	index / set of the planning stage	l / \mathcal{L}	index / set of energy types
m / \mathcal{Y}	index / set of years	t / \mathcal{T}	index / set of time step
d / \mathcal{D}	index / set of days	s / \mathcal{S}	index / set of scenarios
$i, j / \mathcal{I}$	index / set of candidate equipment		

Parameters and Constants

$m_{i,j}$	investment year of equipment i, j	MC	marginal cost
$\zeta_{i,j}$	degradation coefficient of equipment i, j	ΔC^{th}	upper limits of cost fluctuations
$\eta_{i,j}$	initial efficiency of equipment i, j	$C_{i,j,m}^{\text{slvg}}$	salvage value of equipment i, j in year m
$\eta_{i,j,m}$	efficiency of equipment i, j in year m	$C_{i,j,m}^{\text{inv}}$	investment cost of equipment i, j in year m
$\alpha, \beta, \gamma, \delta,$ ε	cycle aging coefficients	$C_{i,j,m}^{\text{dep}}$	annual depreciation cost of equipment i, j
θ, E_{as}, R	calendar aging coefficients defining an Arrhenius factor	$Y_{i,j}^{\text{life}}$	lifespan of equipment i, j
$K_{d,m}$	the average surrounding temperature	$\rho_{i,j}$	salvage value rate of equipment i, j
L	total duration in days	PR_m	present value factor for year m
$\sigma_{d,m}^{\text{ES}}$	capacity loss of ES on day d	$C_{t,m,p}^e$	electricity price at time t, m in stage p
$S_{d,m}^{\text{ES,max}}$	capacity of ES on day d	$C_{t,m,p}^g$	nature gas price at time t, m in stage p
$S_{t,d,m}^{\text{TS,Loss}}$	capacity loss of TS at time t, d, m	$C_{i,j}^{\text{on}}$	maintenance cost of equipment i, j
ζ^{TS}	degradation coefficient of TS	λ_l	load shedding cost for load type l
$\eta^{\text{TS,dis}}$	discharging efficiency of TS	$c_{m,p}^{\text{emi}}$	carbon emission cost
$\eta^{\text{TS,ch}}$	charging efficiency of TS	$N_{i,p}^{\text{max/min}}$	max/ min configuration quantity
θ^{storage}	self-discharge loss of TS	$P_p^{\text{grid,max}}$	max power exchange with the grid
θ^{static}	static loss coefficient of TS	$F_p^{\text{gas,max}}$	max power exchange with gas network
$S_{t,d,m}^{\text{TS,unuse}}$	unused energy of TS at time t, d, m	$P_{i,j}^{\text{min/max}}$	max /min power of equipment i, j
$S^{\text{TS,max}}$	the capacity of TS	$L_{l,t,d,m,p}$	energy demand for load type l
$K^{\text{TS,max}}$	maximum temperatures of TS	$C_{\alpha\beta}^{\text{inv}}$	cost vector of existing equipment
$K^{\text{TS,min}}$	minimum temperatures of TS	$C_{\alpha\beta}^{\text{rep}}$	cost vector of new equipment
$\mu_{i,j}$	reliability degradation coefficient	T_0 / T_s	coefficient matrix associated with \mathbf{x}
$T_{i,j}^{\text{end}}, Y_{i,j}^{\text{end}}$	lifespan time of equipment i, j	\mathbf{b}_0	right-hand side vector associated with \mathbf{x}
$f_{i,j,t,d,m}$	failure rate for equipment i, j	\mathbf{c}_0	cost vector associated with \mathbf{x}
ΔP	variation of uncertain parameters	\mathbf{b}_s	right-hand side vector associated with \mathbf{y}_s
MB	marginal benefit	\mathbf{W}_s	coefficient matrix associated with \mathbf{y}_s

Variables*

$P_{t,d,m}^{\text{ES,ch}}$	charging power of ES at time t, d, m	C_p^{rep}	replacement cost in stage p
$Q_{t,d,m}^{\text{TS,ch}}$	charging power of TS at time t, d, m	$P_{i,j,t,d,m,p}$	output power of equipment i, j

$Q_{t,d,m}^{TS,dis}$	discharging power of TS at time t, d, m	$F_{t,d,m,p}^{gas}$	output gas flow of equipment i, j
$S_{t,d,m}^{TS}$	thermal energy of TS at time t, d, m	$P_{t,d,m,p}^{grid}$	power exchange between grid and ICES
C_p^{total}	total cost in stage p	$P_{t,d,m,p}^{grid\pm}$	power exchange between grid and ICES
C_p^{inv}	investment cost in stage p	$R_{l,t,d,m,p}$	load shedding for load l
C_p^{main}	maintenance cost in stage p	$F_{t,d,m,p}$	carbon emission
C_p^{en}	energy cost of stage p	y_p^{dev}	operating variables of existing equipment
C_p^{rel}	reliability cost in stage p	y_p^{rep}	operating variables of new equipment
C_p^{emi}	carbon emission cost in stage p	θ	slack variable of the subproblem
C_p^{slvg}	salvage value in stage p		

52 * The domain of all variables in this table is $\mathbb{R}_{\geq 0} = \{x \in \mathbb{R} | x \geq 0\}$.

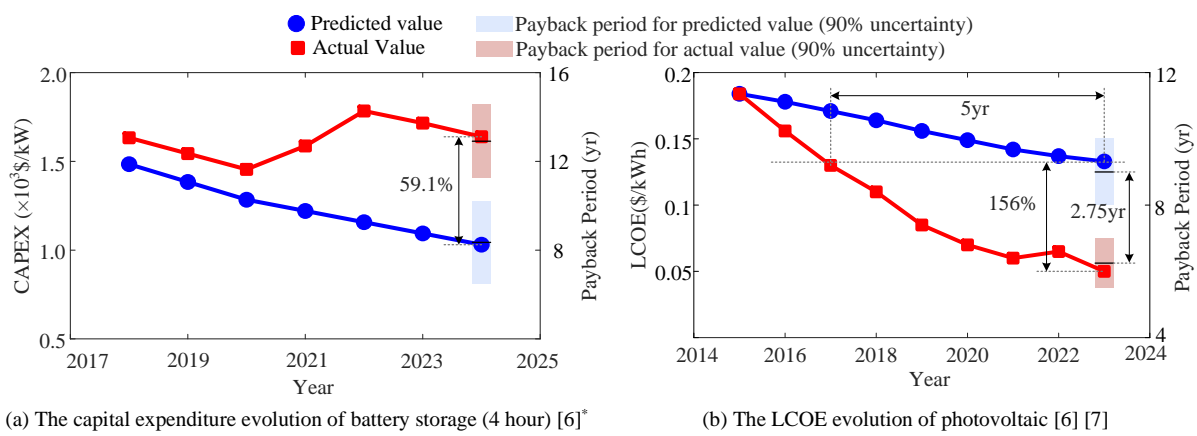
53 1. Introduction

54 In response to the growing energy crises and worsening greenhouse effect, building a reliable, low-carbon
55 energy system is more urgent than ever [1][2]. An integrated community energy system (ICES), by incorporating
56 multiple energy forms such as electricity, heat, and gas, fostering renewable energy consumption, and mitigating
57 greenhouse gas emissions[3]-[5]. Therefore, effective planning of an ICES is critical to addressing current energy
58 and environmental challenges.

59 The performance of ICES planning models depends on accurate predictions of uncertain parameters. However,
60 unpredictable events make this task highly challenging. For example, battery storage has seen limited cost
61 reductions due to rising raw material prices, with deviations reaching 59.1% from the forecasted values, as shown
62 in Fig. 1. Meanwhile, policy-driven initiatives have led to a more than threefold drop in the levelized cost of
63 electricity (LCOE) of photovoltaics (PV) over the past decade, resulting in a 156% deviation from estimates by the
64 National Renewable Energy Laboratory [6]. This discrepancy has caused an average 2.75-year difference in the
65 payback period for photovoltaic projects. Therefore, in long-term energy planning, predictions of load growth,
66 energy prices, and technological evolution are critical and cannot be overlooked. Significant forecasting errors
67 caused by unpredictable events could lead to substantial economic losses and security risks.

68 However, single-stage planning (SSP) often assumes static parameters throughout the planning horizon, leading
69 to early-stage developments that fail to adequately account for future uncertainties [8]-[10]. Over time, load growth,
70 technological advancements, and fluctuations in energy prices exacerbate both operational energy risks and
71 economic risks [11]. To address these limitations, multi-stage planning (MSP) models have been developed for
72 ICES [14]-[18]. Notably, the method presented in [19] for long-term power system planning effectively accounts
73 for the intermittency of renewable energy, ensuring that both initial and subsequent expansion plans are well-

74 coordinated. A stochastic MSP model is proposed to optimize both economic and carbon emission costs,
 75 incorporating the effects of short-term forecasting errors [9]. However, while models like MANGO [8] consider
 76 dynamic factors such as equipment prices, technological advancements, and equipment degradation, they fail to
 77 handle unpredictable events. The impact of technological advancements is often underestimated in existing studies.
 78 with some studies focusing primarily on equipment costs, prematurely discarding older technologies when new
 79 ones provide only marginal improvements [8]. Moreover, many studies [8] [9] assume fixed planning periods for
 80 each stage, which fails to capture the unpredictable nature of real-world ICES planning.



81 **Fig. 1** The price evolution of battery storage and PV

82 The concept of event-driven strategies in manage unpredictable events is inspired by control theory. Rather than
 83 optimizing at every time step, actions are triggered only when specific events occur. These events are typically
 84 identified using methods such as infinitesimal perturbation analysis [20], differential analysis [21], and threshold-
 85 based approaches [22]. However, these techniques fail to quantify the cost impacts of unpredictable events.
 86 Marginal cost analysis, in contrast, quantifies both the marginal costs and benefits, offering a more effective event-
 87 driven approach [23]. As shown in Fig. 1(b), using 2023 forecasted photovoltaic LCOE as the investment point,
 88 the event-driven strategy allows planning 5 years earlier, thereby increasing economic returns.

89 Moreover, accurate simulation of operating conditions is essential to improve planning accuracy. However, the
 90 impact of renewable energy fluctuations and random equipment failures on operational costs and reliability is
 91 substantial. Therefore, it is necessary to account for these factors during the planning process. Recently, an

* The payback period for battery storages is calculated based on a business model that takes advantage of peak and off-peak electricity pricing.

92 advanced method for quantifying renewable energy fluctuations involves using 8,760-hour scenario simulations,
93 while random equipment failures are quantified through reliability analysis. However, reliability is often treated as
94 a hard constraint [24], separate from economic planning. This traditional approach begins with economic planning,
95 followed by a reliability assessment, which can result in suboptimal trade-offs between economy and reliability.
96 Although methods have been developed to directly integrate reliability into the planning model [25] [26], the heavy
97 computational burden of reliability analysis limits the effectiveness.

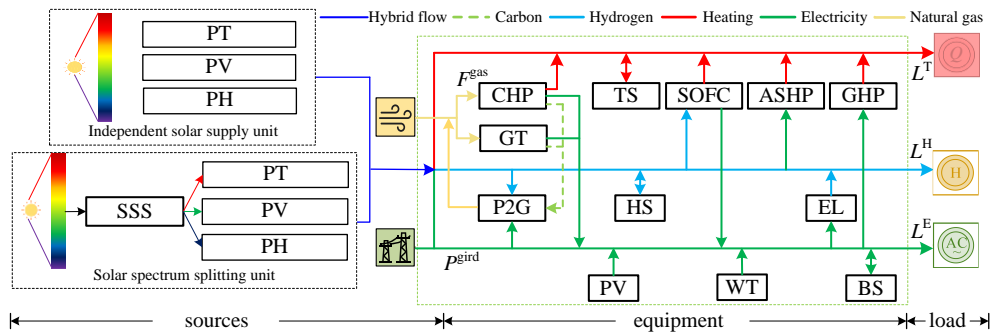
98 To address these challenges, a hybrid time-and-event-driven multi-stage planning (HTED-MSP) model is
99 proposed for ICES. In HTED-MSP model, unpredictable events can be manifested through forecasting errors in
100 load growth, energy prices, and technological development. When forecasting errors exceed the threshold
101 determined by marginal cost analysis, the event-driven strategy is triggered, prompting an early transition to the
102 next planning stage. However, even forecasting errors are small, planning adjustments are still necessary, as factors
103 like equipment aging can reduce system reliability. To address this, a time-driven strategy is proposed to enhance
104 the reliability of ICES. Furthermore, HTED-MSP incorporates 8,760-hour normal and $N-k$ contingency scenarios
105 to accurately simulate the impact of renewable energy variability and equipment failures on reliability. To alleviate
106 the computational burden, the HTED-MSP model is first divided into a simplified MILP sub-model and a large-
107 scale LP operational sub-model with massive scenarios. A State Similarity (SS) method is then proposed, which
108 captures parameter variations across different scenarios and converts them into parameter fluctuations in multi-
109 parameter optimization, generating critical regions (CR). By leveraging positions of optimal bases (POB) to express
110 similar features across different scenarios, SS simplifies all optimization scenarios within each critical region into
111 linear equation solving, enabling rapid scenario analysis. The main contributions are as follows:

- 112 ● A Hybrid Time-and-Event-Driven Multi-Stage Planning (HTED-MSP) model is proposed. The event-
113 driven strategy mitigates economic risks from forecasting errors using a marginal cost-based trigger
114 mechanism, while the time-driven strategy enhances operational reliability.
- 115 ● A state-similarity-based scenario analysis method is proposed to accelerate MILP problem solving. By
116 reusing the POB of linear subproblems, optimization iterations for scenarios with the same POB are
117 transformed into equation solving. This approach enhances the efficiency of large-scale scenario analysis
118 in ICES planning while maintaining result accuracy.

119 The rest of this paper is structured as follows: Section 2 establishes the ICES model. Section 3 develops the
 120 HTED-MSP model, detailing the time-driven and event-driven strategies, along with the RTR. Section 4 formulates
 121 the HTED-MSP as a two-stage MILP model and introduces the SS method. Section 5 presents a case study to
 122 demonstrate the effectiveness of the proposed methods. Finally, Section 6 concludes the paper.

123 2. ICES Modelling

124 This section presents detailed models of equipment operation, degradation, and reliability for ICES planning.
 125 Fig. 2 illustrates the typical configuration of an ICES. The system comprises various components, including energy
 126 conversion equipment (such as CHP, SOFC, and EL), renewable energy sources (PV and WT), energy storage units
 127 (BS, TS, and HS), Power-to-Gas systems (P2G and CCS), and diverse loads. In addition, the ICES framework
 128 incorporates promising technologies, including innovative but currently costly solutions, such as solar spectral
 129 splitting (SSS) for thermo-electro-hydrogen production systems [27] [28].



130
131 **Fig. 2** Typical ICES system structure

132 2.1. Equipment Operation Model

133 ICES efficiently utilizes electricity and natural gas to meet electrical, thermal, and hydrogen demands. All the
 134 equipment operation models are discussed in Appendix A.

135 2.2. Equipment Degradation Model

136 2.2.1 Degradation models of energy conversion equipment

137 For energy conversion equipment, the degradation model can be formulated to reflect the decline in energy
 138 conversion efficiency. The equipment efficiency can be adjusted as follows:

$$139 \eta_{i,j,m} = (1 - \xi_{i,j})^{m - m_{i,j}} \eta_{i,j} \quad \forall i, j \in \mathcal{I}, m \in \mathcal{Y} \quad (1)$$

140 *2.2.2 Degradation model for electricity storage*

141 The aging of ES includes both calendar aging and cyclic aging. Calendar aging occurs over time and is primarily
 142 influenced by factors such as temperature and environmental conditions, while cyclic aging results from the
 143 charging and discharging cycles. The HTED-MSP integrates a capacity loss model for lithium-ion batteries,
 144 considering both calendar aging and cyclic aging [29] [30].

$$145 \quad \sigma_{d,m}^{\text{ES}} = (\alpha K_{d,m}^2 + \beta K_{d,m} + \gamma) \varepsilon^{(\delta K_{d,m} + \varepsilon)} \sum_{t \in [d-1, d]} P_{t,d,m}^{\text{ES, ch}} + \theta \varepsilon^{-E_a \sqrt{L} / R K_{d,m}} \quad \forall d \in \mathcal{D}, m \in \mathcal{Y} \quad (2)$$

$$146 \quad S_{d+1,m}^{\text{ES, max}} = S_{d,m}^{\text{ES, max}} (1 - \sigma_{d,m}^{\text{ES}}) \quad \forall d \in \mathcal{D}, m \in \mathcal{Y} \quad (3)$$

147 *2.2.3 Degradation model for thermal storage*

148 Thermal energy loss in TS primarily occurs due to heat conduction, as heat naturally flows from higher to lower
 149 temperatures [31]. The insulation performance of TS systems may degrade due to aging materials, physical damage,
 150 or prolonged thermal stress, leading to daily thermal energy loss. The insulation degradation model, based on the
 151 operational model in Appendix A.2, can be integrated into the TS model.

$$152 \quad S_{t,d,m}^{\text{TS}} = S_{t-1,d,m}^{\text{TS}} + \eta^{\text{TS, ch}} Q_{t,d,m}^{\text{TS, ch}} - Q_{t,d,m}^{\text{TS, dis}} / \eta^{\text{TS, dis}} - S_{t,d,m}^{\text{TS, Loss}} \quad \forall t \in \mathcal{T}, d \in \mathcal{D}, m \in \mathcal{Y} \quad (4)$$

$$153 \quad S_{t,d,m}^{\text{TS, Loss}} = S_{t-1,d,m}^{\text{TS}} (1 + \xi^{\text{TS}})^{m - m_i} \theta^{\text{storage}} + S_{t,d,m}^{\text{TS, unuse}} (1 + \xi^{\text{TS}})^{m - m_i} \theta^{\text{static}} \quad \forall t \in \mathcal{T}, d \in \mathcal{D}, m \in \mathcal{Y} \quad (5)$$

$$154 \quad S_{t,d,m}^{\text{TS, unuse}} = S^{\text{TS, max}} (K^{\text{TS, min}} - K_{t,d,m}) / (K^{\text{TS, max}} - K^{\text{TS, min}}) \quad \forall t \in \mathcal{T}, d \in \mathcal{D}, m \in \mathcal{Y} \quad (6)$$

155 **2.3. Equipment Reliability Model**

156 The reliability model for equipment is designed to accurately simulate its performance under actual operational
 157 conditions. The time-dependent ‘‘Failure Rate’’ is directly employed as the standard metric for measuring equipment
 158 reliability [32]. Typically, the failure rate increases gradually with the usage.

$$159 \quad f_{i,j,t,d,m} = \left(1 + (t / T_{i,j}^{\text{life}})^{\mu_{i,j}}\right) f_{i,j,t=0,d,m} \quad \forall i, j \in \mathcal{I}, t \in \mathcal{T}, d \in \mathcal{D}, m \in \mathcal{Y} \quad (7)$$

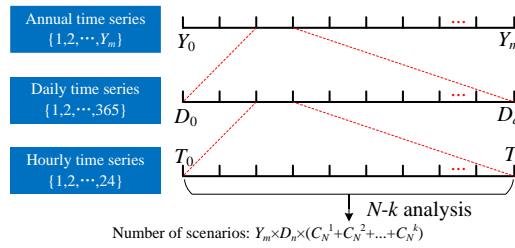
160 However, within a single optimization year, the failure rate typically increases at a minimal rate. Consequently,
 161 this paper assumes a constant failure rate for each optimization year. The failure rate can be approximated as follows:

$$162 \quad f_{i,j,m} = \left(1 + (m / Y_{i,j}^{\text{life}})^{\mu_{i,j}}\right) f_{i,j,m=0} \quad \forall i, j \in \mathcal{I}, m \in \mathcal{Y} \quad (8)$$

163 **3. Multi-Stage Planning Model**

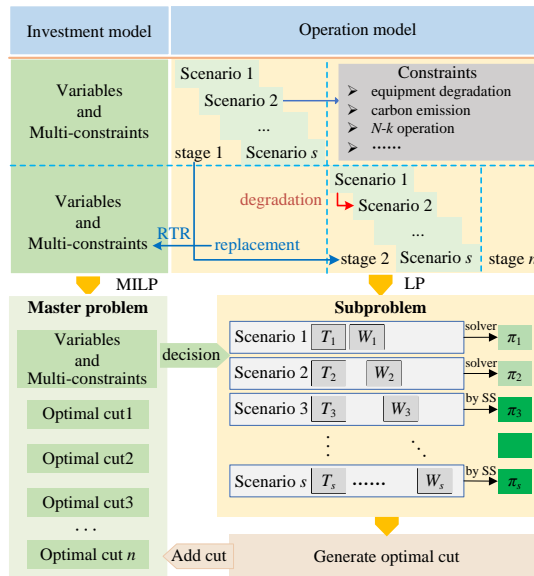
164 Considering the uncertainties in long-term planning, this study establishes a hybrid time-and-event-driven multi-
 165 stage planning (HTED-MSP) model with the following characteristics:

- 166 ● Long-term dynamic trends of load growth, energy prices, and technological advancements are considered,
 167 and an event-driven planning strategy has been implemented based on marginal cost analysis.
- 168 ● Operational analysis is developed based on an 8760-hour framework, with each day optimized over a 24-
 169 hour period, as illustrated in Fig. 3. Temporally correlated operating constraints, such as energy storage
 170 capacity constraints, are incorporated into this framework.
- 171 ● The risks associated with operational uncertainties due to equipment aging and renewable energy
 172 fluctuations are thoroughly evaluated. Operational uncertainties are quantitatively assessed using the $N-k$
 173 operational risk analysis methodology.



174
175

Fig. 3 Temporal horizon representation in the HTED-MSP



176
177

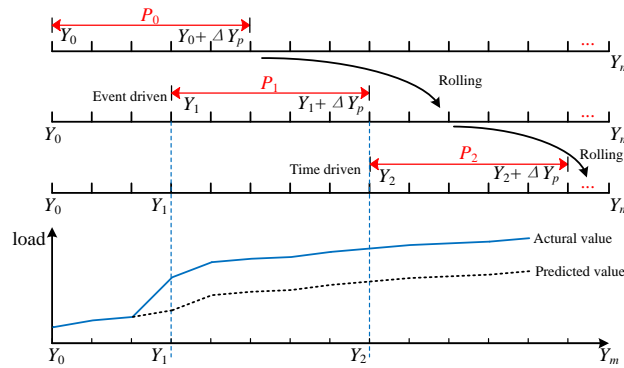
Fig. 4 Structure of the HTED-MSP model

178 As shown in Fig. 4, the HTED-MSP model uses a hybrid time-and-event-driven strategy to determine the start

179 time of each planning stage and employs a two-stage optimization approach. The master problem focuses on
 180 minimizing overall planning costs by optimizing equipment capacity, while the subproblem simulates both normal
 181 and $N-k$ scenarios to minimize operational costs. The $N-k$ contingency scenarios are formulated by enumerating
 182 potential equipment failures based on normal scenarios [33] [34]. Additionally, equipment degradation between
 183 adjacent scenarios is also considered. To prevent frequent equipment replacements caused by the event-driven
 184 strategy, RTR is introduced between planning stages to manage both existing and new equipment. Specifically,
 185 RTR measures implicit and non-economic costs, such as time preferences and risks.

186 3.1. The Hybrid Time and Event-Driven for Multi-Stage Planning

187 Given the significant uncertainty in future conditions, the HTED-MSP model focuses on minimizing costs at
 188 each stage rather than over the entire lifecycle of the ICES. This approach acknowledges the impracticality of long-
 189 term predictions. By using a rolling optimization framework, the HTED-MSP model makes incremental planning
 190 decisions based on the latest information, as shown in Fig. 5. A hybrid time-and-event-driven strategy is proposed
 191 for dynamic stage partitioning, detailed as follows.



192 **Fig. 5** The hybrid time-and-event-driven strategy for HTED-MSP

194 *Event-Driven Strategy:* This strategy is triggered when forecast errors in load growth, energy prices, or technical
 195 parameters exceed a specified threshold, determined through marginal benefit analysis of uncertainty parameters
 196 from the previous planning stage. As shown in Eq. (9), the event-driven mechanism is triggered when the difference
 197 between marginal benefits and marginal costs exceeds a critical value. Marginal benefits refer to the additional
 198 gains from adjusting the plan, while marginal costs represent the extra expenses incurred by implementing the
 199 adjustment. As illustrated in Fig. 5, stage P_1 represents an event-driven phase activated by significant forecast errors.
 200 Notably, ICES expansion plans can also be considered event driven.

$$201 \quad MB(\Delta P) - MC(\Delta P) \geq \Delta C^{\text{th}} \quad (9)$$

202 *Time-Driven Strategy*: When the impact of unpredictable events is not significant, the event-driven strategy is
 203 not triggered. However, planning adjustments are still needed due to increased operational risks from equipment
 204 aging. Therefore, a time-driven planning strategy is introduced, as illustrated by stage P_2 in Fig. 5.

205 3.2. Model Formulation

206 3.2.1 Objective functions

207 The HTED-MSP model aims to minimize total costs of investment, maintenance, energy, reliability, CO₂
 208 emissions, and replacement at each stage.

$$209 \quad \min C_p = C_p^{\text{total}} + C_p^{\text{rep}} \quad \forall p \in \mathcal{P} \quad (10)$$

$$210 \quad C_p^{\text{total}} = C_p^{\text{inv}} + C_p^{\text{main}} + C_p^{\text{en}} + C_p^{\text{rel}} + C_p^{\text{emi}} \quad \forall p \in \mathcal{P} \quad (11)$$

$$211 \quad C_p^{\text{inv}} = \sum_{i \in \mathcal{I}} (N_{i,p}^{\text{inv}} - N_{i,p-1}^{\text{inv}} + N_{i,p}^{\text{rep}}) c_{i,m_p}^{\text{inv}} + \sum_{i \in \mathcal{I}} \sum_{j \in [0, N_{i,p-1}^{\text{inv}} - N_{i,p}^{\text{rep}}]} C_{i,j,m_p}^{\text{slvg}} - C_p^{\text{slvg}} \quad \forall m \in \mathcal{Y}, p \in \mathcal{P} \quad (12)$$

$$212 \quad C_p^{\text{slvg}} = \sum_{i \in \mathcal{I}} \sum_{j \in [0, N_{i,p}^{\text{inv}}]} \left(C_{i,j,m_p}^{\text{slvg}} - \sum_{m \in [m_p, m_{p+1}-1]} C_{i,j,m}^{\text{dep}} \right) \quad \forall p \in \mathcal{P} \quad (13)$$

$$213 \quad C_{i,j,m}^{\text{dep}} = c_{i,j,m_i,j}^{\text{inv}} (1 - \rho_{i,j}) / Y_{i,j}^{\text{life}} \quad \forall i, j \in \mathcal{I}, m \in \mathcal{Y} \quad (14)$$

$$214 \quad C_{i,j,m_p}^{\text{slvg}} = c_{i,j,m_i,j}^{\text{inv}} - \sum_{m \in [m_i,j, m_p]} C_{i,j,m}^{\text{dep}} \quad \forall i, j \in \mathcal{I}, p \in \mathcal{P} \quad (15)$$

$$215 \quad C_p^{\text{main}} = \sum_{i,j \in \mathcal{I}} \sum_{j \in [0, N_{i,p}^{\text{inv}}]} \sum_{t \in \mathcal{T}, d \in \mathcal{D}, m \in \mathcal{Y}} PR_m \cdot c_{i,j}^{\text{om}} P_{i,j,t,d,m,p} \quad \forall p \in \mathcal{P} \quad (16)$$

$$216 \quad C_p^{\text{en}} = \sum_{t \in \mathcal{T}, d \in \mathcal{D}, m \in \mathcal{Y}} PR_m \cdot (c_{t,m,p}^{\text{e}} P_{t,d,m,p}^{\text{gird}} + c_{t,m,p}^{\text{g}} F_{t,d,m,p}^{\text{gas}}) \quad \forall p \in \mathcal{P} \quad (17)$$

$$217 \quad C_p^{\text{rel}} = \sum_{l \in \mathcal{L}} \sum_{t \in \mathcal{T}, d \in \mathcal{D}, m \in \mathcal{Y}} PR_m \cdot \lambda_l R_{l,t,d,m,p} \quad \forall p \in \mathcal{P} \quad (18)$$

$$218 \quad C_p^{\text{emi}} = \sum_{t \in \mathcal{T}, d \in \mathcal{D}, m \in \mathcal{Y}} PR_m \cdot c_{m,p}^{\text{emi}} F_{t,d,m,p} \quad \forall p \in \mathcal{P} \quad (19)$$

219 where variables $N_{i,p}^{\text{inv}} \in \mathbb{N}$ and $N_{i,p}^{\text{rep}} \in \mathbb{N}$ represent the configuration quantity and the replacement quantity of
 220 equipment i, j , respectively. Eq. (12) shows that the investment cost of equipment consists of two components: the
 221 cost of new equipment and the recovery cost. The recovery cost is defined as the difference between the salvage
 222 value of unreplaced equipment and the total salvage value of all equipment. Eq. (13) calculates the total salvage
 223 value of all equipment, while Eq. (14) defines the annual depreciation cost of equipment i, j . Finally, Eq. (15)

224 provides the salvage value of equipment i, j in year m .

225 The replacement cost C_p^{rep} can be calculated as the difference between the cost of new equipment and the salvage
226 value of the old equipment.

$$227 \quad C_p^{\text{rep}} = \sum_{i,j \in \mathcal{I}} \sum_{j \in \{0, N_{i,p}^{\text{rep}}\}} (c_{i,j,m_p}^{\text{inv}} - C_{i,j,m_p}^{\text{slvg}}) \quad \forall m \in \mathcal{Y}, p \in \mathcal{P} \quad (20)$$

228 3.2.2 Constraints

$$229 \quad N_{i,p}^{\text{min}} \leq N_{i,p}^{\text{inv}} \leq N_{i,p}^{\text{max}} \quad \forall i \in \mathcal{I}, p \in \mathcal{P} \quad (21)$$

$$230 \quad 0 \leq N_{i,p}^{\text{rep}} \leq N_{i,p-1}^{\text{inv}} \quad \forall i \in \mathcal{I}, p \in \mathcal{P} \quad (22)$$

$$231 \quad -P_p^{\text{grid,max}} \leq P_{t,d,m,p}^{\text{grid}} \leq P_p^{\text{grid,max}} \quad \forall t \in \mathcal{T}, d \in \mathcal{D}, m \in \mathcal{Y}, p \in \mathcal{P} \quad (23)$$

$$232 \quad 0 \leq F_{t,d,m,p}^{\text{gas}} \leq F_p^{\text{gas,max}} \quad \forall t \in \mathcal{T}, d \in \mathcal{D}, m \in \mathcal{Y}, p \in \mathcal{P} \quad (24)$$

$$233 \quad P_{i,j}^{\text{min}} \leq P_{i,j,t,d,m,p} \leq P_{i,j}^{\text{max}} \quad \forall i, j \in \mathcal{I}, t \in \mathcal{T}, d \in \mathcal{D}, m \in \mathcal{Y}, p \in \mathcal{P} \quad (25)$$

$$234 \quad 0 \leq R_{l,t,d,m,p} \leq L_{l,t,d,m,p} \quad \forall l \in \mathcal{L}, t \in \mathcal{T}, d \in \mathcal{D}, m \in \mathcal{Y}, p \in \mathcal{P} \quad (26)$$

235 Eqs. (21) and (22) define scale limitations, while (23) to (26) formulate ICES box constraints. It should be noted
236 that constraints (23) can be transformed using (27)-(29) to ensure that all variables of HTED-MSP remain non-
237 negative.

$$238 \quad P_{t,d,m,p}^{\text{grid}} = P_{t,d,m,p}^{\text{grid+}} - P_{t,d,m,p}^{\text{grid-}} \quad \forall t \in \mathcal{T}, d \in \mathcal{D}, m \in \mathcal{Y}, p \in \mathcal{P} \quad (27)$$

$$239 \quad 0 \leq P_{t,d,m,p}^{\text{grid+}} \leq P_p^{\text{grid,max}} \quad \forall t \in \mathcal{T}, d \in \mathcal{D}, m \in \mathcal{Y}, p \in \mathcal{P} \quad (28)$$

$$240 \quad 0 \leq P_{t,d,m,p}^{\text{grid-}} \leq P_p^{\text{grid,max}} \quad \forall t \in \mathcal{T}, d \in \mathcal{D}, m \in \mathcal{Y}, p \in \mathcal{P} \quad (29)$$

241 The constraints of the HTED-MSP incorporate the equipment operation, degradation, and reliability models
242 discussed in Section 2. In summary, the HTED-MSP model is formulated as a MILP problem, as represented by
243 Eq. (30).

$$244 \quad \begin{aligned} \min \quad & C_p = C_p^{\text{total}} + C_p^{\text{rep}} \\ & = [\mathbf{c}_\alpha^{\text{inv}}, \mathbf{c}_\alpha^{\text{rep}}]^T [\mathbf{N}_p^{\text{inv}}, \mathbf{N}_p^{\text{rep}}] \\ & + [\mathbf{c}_\beta^{\text{inv}}, \mathbf{c}_\beta^{\text{rep}}]^T [\mathbf{y}_p^{\text{dev}}, \mathbf{y}_p^{\text{rep}}] \\ \text{s.t.} \quad & \left\{ \begin{array}{l} (4) - (6), (11) - (22), (24) - (29), (A1) - (A29) \\ \mathbf{N}_p^{\text{inv}}, \mathbf{N}_p^{\text{rep}} \in \mathbb{N}, \mathbf{y}_p^{\text{dev}}, \mathbf{y}_p^{\text{rep}} \in \mathbb{R}_{\geq 0} \end{array} \right. \end{aligned} \quad (30)$$

245 **3.3. Replacement Threshold Rate**

246 The replacement threshold rate (RTR) is a critical metric in ICES planning, assessing implicit costs (e.g., training
 247 operators for new equipment and the environmental impact of disposing of old equipment) and non-economic costs
 248 (e.g., time preferences and risks). It suggests that existing technologies are not immediately replaced by new ones,
 249 even when the marginal costs of the new technologies are lower, thus ensuring the continued operation of current
 250 technologies. Specifically, an RTR of zero signifies a rapid transition to competitive new equipment, whereas a
 251 high RTR ensures the longevity of existing equipment until the end of its service life. Unlike previous studies, this
 252 paper adopts a holistic approach by considering both the investment and operational costs of equipment as the
 253 criterion for replacement decisions. This comprehensive evaluation method improves decision-making by
 254 accounting for both upfront investments and ongoing operational expenses. Therefore, the revised HTED-MSP
 255 model can be expressed as:

$$\begin{aligned}
 \min \quad & C_p = C_p^{\text{total}} + C_p^{\text{rep}} \\
 & = \left[\mathbf{c}_\alpha^{\text{inv}}, (1 + RTR)\mathbf{c}_\alpha^{\text{rep}} \right]^T \left[\mathbf{N}_p^{\text{inv}}, \mathbf{N}_p^{\text{rep}} \right] \\
 & + \left[\mathbf{c}_\beta^{\text{inv}}, (1 + RTR)\mathbf{c}_\alpha^{\text{rep}} \right]^T \left[\mathbf{y}_p^{\text{dev}}, \mathbf{y}_p^{\text{rep}} \right] \\
 \text{s.t.} \quad & \left\{ \begin{array}{l} (4) - (6), (11) - (22), (24) - (29), (A1) - (A29) \\ \mathbf{N}_p^{\text{inv}}, \mathbf{N}_p^{\text{rep}} \in \mathbb{N}, \mathbf{y}_p^{\text{dev}}, \mathbf{y}_p^{\text{rep}} \in \mathbb{R}_{\geq 0} \end{array} \right.
 \end{aligned} \tag{31}$$

257 **4. Solution Framework for the HTED-MSP Model**

258 The HTED-MSP model is compactly formulated using matrix notation, with scenarios quantified daily. For any
 259 given stage p and scenario s , the model (31) is expressed as follows:

$$\begin{aligned}
 \min \quad & C_p = \mathbf{c}_0^T \mathbf{x} + \sum_{s \in \mathcal{S}} p_s \cdot \mathbf{c}_s^T \mathbf{y}_s \\
 \text{s.t.} \quad & \begin{bmatrix} \mathbf{T}_0 & 0 \\ \mathbf{T}_s & \mathbf{W}_s \end{bmatrix} \begin{bmatrix} \mathbf{x} \\ \mathbf{y}_s \end{bmatrix} = \begin{bmatrix} \mathbf{b}_0 \\ \mathbf{b}_s \end{bmatrix} \quad \forall s \in \mathcal{S}, \mathbf{x} \in \mathbb{N}, \mathbf{y}_s \in \mathbb{R}_{\geq 0}
 \end{aligned} \tag{32}$$

261 where \mathbf{x} represents all binary and integer variables, \mathcal{S} denotes the set of scenarios, including hourly normal scenarios
 262 and $N-k$ contingency scenarios. while \mathbf{y}_s denotes the continuous variables for scenario s .

263 The scenario set \mathcal{S} and the scenario probabilities p_s are expressed as follows:

$$\mathcal{S} = \left\{ \mathcal{X} \in \{0,1\}^{|\mathcal{I}|} \mid \sum_{i,j \in \mathcal{I}} \mathcal{X}_{i,j} \leq k \right\} \times \mathcal{D} \times \mathcal{Y} \tag{33}$$

265
$$p_s = \prod_{i,j \in \mathcal{I}_n} f_{i,j} \prod_{i,j \in \mathcal{I} \setminus \mathcal{I}_n} (1 - f_{i,j}) \quad \forall s \in \mathcal{S} \quad (34)$$

266 where 0 represents a fault, and 1 indicates normal operation of the equipment. The parameter k denotes the $N-k$
 267 contingency level, specifying the number of simultaneous faults being considered. $f_{i,j}$ is determined by (8), and \mathcal{I}_n
 268 represents the set of faulty equipment.

269 Considering the 365 scenario simulations in a year and the $N-k$ contingency scenarios, Eq. (32) is a large-scale
 270 MILP problem. In this study, the L-shaped algorithm [35] is introduced to transform the HTED-MSP model into a
 271 two-stage optimization model. Then, a state similarity (SS) method is proposed to alleviate the computational
 272 burden of the HTED-MSP model.

273 **4.1. L-shaped Method**

274 Specifically, the L-shaped algorithm formulates the model (32) as a master problem and a multitude of
 275 subproblems. The master problem includes all integer and binary variables, forming a mixed-integer programming
 276 problem, while the subproblems are linear programming problems. As shown in Fig. 4, once the master problem
 277 decision variables \mathbf{x} is determined, all the subproblems can be solved separately.

278 For a given decision variable \mathbf{x}^v in the master problem, the subproblem is formulated as:

279
$$\begin{aligned} \min_{\mathbf{y}_s} \quad & \omega = p_s \cdot \mathbf{c}_s^T \mathbf{y}_s \\ \text{s.t.} \quad & \mathbf{T}_s \mathbf{x}^v + \mathbf{W}_s \mathbf{y}_s = \mathbf{b}_s : \boldsymbol{\pi}_s^v \\ & \forall s \in \mathcal{S}, \mathbf{y}_s^v \in \mathbb{R}_{\geq 0} \end{aligned} \quad (35)$$

280 where v is the iteration counter. $\boldsymbol{\pi}_s^v \in \mathbb{R}$ is the dual variable associated with scenario s . The optimal solution to the
 281 subproblem is the sum of the minimum operation costs across all scenarios. By introducing the slack variable θ ,
 282 the investment master problem is formulated as:

283
$$\begin{aligned} \min_{\mathbf{x}} \quad & \mathbf{C}_p = \mathbf{c}_0^T \mathbf{x} + \theta^v \\ \text{s.t.} \quad & \begin{cases} \mathbf{T}_0 \mathbf{x}^v = \mathbf{b}_0 \\ \theta^v \geq e^l - \mathbf{E}^l \mathbf{x} \\ \mathbf{x} \in \mathbb{N}, \theta^v \in \mathbb{R}_{\geq 0}, l \in \{1, \dots, v\} \end{cases} \end{aligned} \quad (36)$$

284 where the constraint $\theta^v \geq e^l - \mathbf{E}^l \mathbf{x}$ is called the optimal cut. The rigorous mathematical expression for the optimal
 285 cut in the L-shaped method can be found in [36]. Define

286

$$\begin{aligned}
e^v &= \sum p_s \cdot (\boldsymbol{\pi}_s^v)^T \mathbf{b}_s \quad \forall s \in \mathcal{S} \\
\mathbf{E}^v &= \sum p_s \cdot (\boldsymbol{\pi}_s^v)^T \mathbf{T}_s \quad \forall s \in \mathcal{S}
\end{aligned} \tag{37}$$

287 Let $\omega^v = e^v - \mathbf{E}^v \mathbf{x}^v$. If $\theta^v \geq \omega^v$, the process stops; otherwise, the optimal cut is added to Eq. (36).

288 4.2. Scenario Analysis Method Based on State Similarity

289 When solving the scenario-based two-stage problem, the numerous sub-problems lead to a significant
290 computational burden. To address this, a state-similarity-based scenario analysis method is proposed to enhance
291 the solution efficiency.

292 The SS method is inspired by multi-parametric linear programming (MPLP) [37], where the positions of the
293 optimal basis matrix (POB) for all states within the same critical region are consistent. This implies that when using
294 the simplex method [38] for optimization, linear problems can be directly solved using POB equations instead of
295 iterative optimization.

296 Therefore, the SS method has the following characteristics:

- 297 ● The SS method classifies scenarios based on POB, and the classification results are dynamic, depending
298 on the boundary conditions of the main and sub-problems.
- 299 ● Solving POB-based equations replaces iterative optimization while maintaining the optimality of the linear
300 problems.

301 The differences between various sub-scenario models lie in load levels, renewable energy levels, energy prices,
302 equipment parameters, and the operational status of the equipment. These differences are specifically reflected in
303 the model (35), expressed as variations in \mathbf{c}_s , \mathbf{b}_s , and \mathbf{W}_s . The standard multi-parametric planning form of the model
304 (35) is expressed as:

$$\begin{aligned}
\min_{\mathbf{y}} \omega &= p [\mathbf{c} + \boldsymbol{\delta}_c]^T \mathbf{y}^v \\
\text{s.t. } & [\mathbf{T} + \boldsymbol{\delta}_T] \mathbf{x} + [\mathbf{W} + \boldsymbol{\delta}_W] \mathbf{y}^v = [\mathbf{b} + \boldsymbol{\delta}_b]: \boldsymbol{\pi}^v \mathbf{y}^v \in \mathbb{R}_{\geq 0}
\end{aligned} \tag{38}$$

306 where $\boldsymbol{\delta}_c$, $\boldsymbol{\delta}_b$, $\boldsymbol{\delta}_T$, and $\boldsymbol{\delta}_W$ represent variations in energy prices, load demands, equipment states, and equipment
307 parameters.

308 In the model (38), the optimization variables that form the vertices of the feasible region are designated as *basic*
309 *variables*, and the coefficient matrix associated with these basic variables is designated as the *basis matrix*. *Non-*

310 *basic variables*, which are set to zero in a vertex solution, are associated with the *non-basis matrix*. When the model
 311 achieves an optimal solution, the *basic variables* and the *basis matrix* become the *optimal basic variables* and the
 312 *optimal basis matrix*. Clearly, the optimal basis matrix and the POB are in one-to-one correspondence.

313 Then, the subproblem model (38) can be divided into the *basic matrix* and the corresponding *non-basis matrix*
 314 forms, as follows:

$$315 \quad \min_{\mathbf{y}} \omega = p \left[\mathbf{c}_B + \boldsymbol{\delta}_{c_B} \quad \mathbf{c}_N + \boldsymbol{\delta}_{c_N} \right]^T \mathbf{y}^v \quad (39)$$

$$\text{s.t. } [\mathbf{T} + \boldsymbol{\delta}_T] \mathbf{x} + \left[\mathbf{W}_B + \boldsymbol{\delta}_{W_B} \quad \mathbf{W}_N + \boldsymbol{\delta}_{W_N} \right] \mathbf{y}^v = [\mathbf{b} + \boldsymbol{\delta}_b] : \boldsymbol{\pi}^v \quad \mathbf{y}^v \in \mathbb{R}_{\geq 0}$$

316 where B and N respectively represent *basic* and *non-basis* parameters. According to the simplex theory, the
 317 necessary and sufficient condition for maintaining an unchanged *optimal basis* is to satisfy the following constraints:

$$318 \quad \left(\mathbf{W}_B + \boldsymbol{\delta}_{W_B} \right)^{-1} \left[\mathbf{b} + \boldsymbol{\delta}_b - [\mathbf{T} + \boldsymbol{\delta}_T] \mathbf{x}^v \right] \geq \mathbf{0} \quad (40)$$

$$319 \quad \left[\mathbf{c}_N + \boldsymbol{\delta}_{c_N} \right]^T - \boldsymbol{\pi}^v \left[\mathbf{W}_N + \boldsymbol{\delta}_{W_N} \right] \geq \mathbf{0} \quad (41)$$

320 A group of SS-Sets is defined to classify subproblem scenarios with similarities. Therefore, all subproblems
 321 within the same SS-Set can be represented using the same POB. The optimal solution for the SS set is obtained by:

$$322 \quad \omega^v = (\mathbf{c}_B + \boldsymbol{\delta}_{c_B}) \left(\mathbf{W}_B + \boldsymbol{\delta}_{W_B} \right)^{-1} \left([\mathbf{b} + \boldsymbol{\delta}_b] - [\mathbf{T} + \boldsymbol{\delta}_T] \mathbf{x}^v \right) \quad (42)$$

323 Based on the SS-Set, determine if subsequent subproblems belong to the SS-Set using Eqs. (40) and (41). If so,
 324 the optimal solution can be directly obtained through Eq. (42). If not, solve the subproblem using a commercial
 325 solver and generate a new SS-Set. Repeat this process until all subproblems are solved.

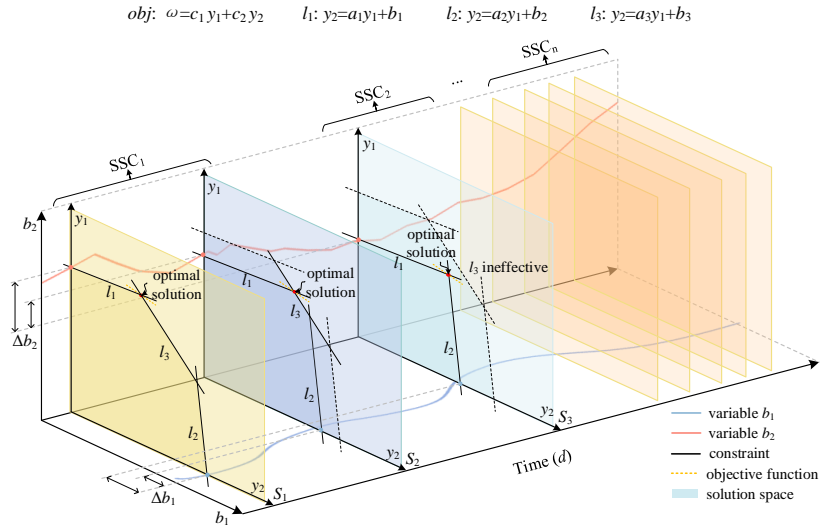


Fig. 6 Two-dimensional description of the SS method solution process.

326
327

328 As shown in Fig. 6, b_1 and b_2 are parameter variables in constraints l_1 , l_2 , and l_3 , with their fluctuation ranges
 329 indicated by the red and blue lines, respectively. S_1 , S_2 , and S_3 represent the feasible regions formed by three sets
 330 of parameter variables. Since scenarios S_1 and S_2 have the same POB, these two scenarios are considered similar.
 331 This implies that the optimal solution for S_2 can be quickly obtained using (42). In contrast, the POB for S_3 differs
 332 from that of S_1 , requiring an optimization process to determine its solution. Therefore, the SS method leverages the
 333 mathematical characteristics of subproblem solutions to classify a large number of optimization problems,
 334 simplifying them into matrix multiplication. However, this simplification does not compromise the optimality of
 335 the solutions.

336 5. Case Study

337 5.1. System Description

338 To evaluate the proposed HTED-MSP model, a case study was conducted in an ICES, as shown in Fig. 2. The
 339 candidate equipment includes CHP, ASHP, GHP, GT, EL, SOFC, PV, PT, PH, SSS, WT, P2G, and CC. The
 340 equipment failure order $k = 1$. The ICES is interconnected with superior systems via the electrical grid and the
 341 natural gas network. Additionally, it is stipulated that the ICES can purchase electricity from the electrical grid and
 342 sell back surplus power. The P2G system is designed to inject the generated natural gas into the gas network,
 343 exclusively for local energy supply purposes. The planning horizon commenced in 2026 and spanned 30 years.

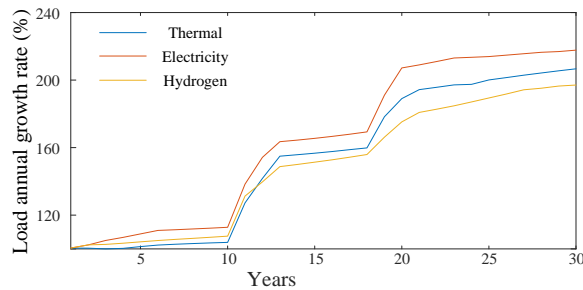
344 The input data for the analysis comprises three categories: i) the energy demand curves; ii) technical and
345 economic parameters of the equipment; and iii) trends in energy prices.

346 i) The load forecast data for 2026-2055 is based on actual data from the ICES and uses the dataset from the
347 "Annual Energy Outlook 2023" [39] to predict the load for the next 30 years. Additionally, two unpredictable events
348 were simulated in years 10 and 18, as shown in Fig. 7.

349 ii) The economic and technical forecast parameters for equipment are derived from the "Assumptions to the
350 Annual Energy Outlook 2023" [40], the SCCER JASM dataset [41], and literature [8] [29] [39] [42]-[45], with
351 detailed information provided in Appendix B. Additionally, the trends in carbon emission parameters for CHP and
352 GT are shown in Fig. 8.

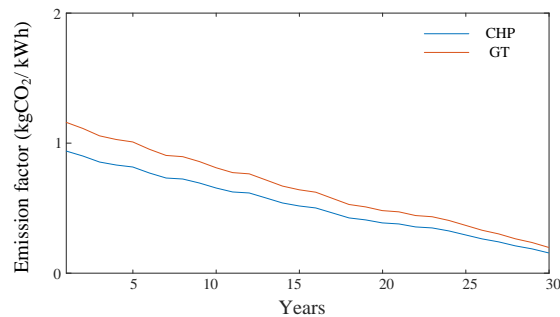
353 iii) Electricity purchase and sale prices, natural gas prices, and the carbon emission index are quantified. The
354 data for the initial year are provided by [43] and [44], whereas forecasts for the future are developed using [8] and
355 [39]. Moreover, 5% forecast errors in natural gas prices were simulated in years 2 and 3.

356 The simulation was run on a standard PC equipped with an Intel Core i5-9400U @1.80GHz CPU and 128.0 GB
357 RAM. Gurobi version 10.0 and Mosek version 9.2 were used in the study.



358
359

Fig. 7 The growth rate curve for heating, electricity, and hydrogen demand (2025 is designated as year 0)



360
361

Fig. 8 The carbon emission factor of CHP and GT

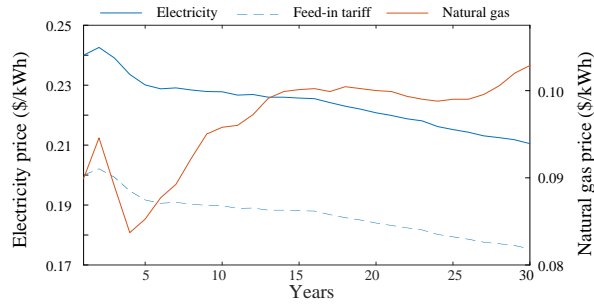


Fig. 9 The energy prices evolutions

362
363

364 **5.2. Results and Comparisons**

365 To validate the effectiveness of the proposed HTED-MSP model, three cases are analyzed: Case A involves a
366 single-stage planning (SSP) strategy, Case B involves a multi-stage planning strategy with a fixed planning period,
367 and Case C focuses on the HTED-MSP strategy. Additionally, the efficacy of the proposed SS method is evaluated
368 by comparing it with the Benders decomposition approach.

Case	2026-2030	2031-2035	2036-2040	2041-2045	2046-2050	2051-2055	
SSP	Stage						
MSP	Stage 1	Stage 2	Stage 3	Stage 4	Stage 5	Stage 6	
HTED	Stage 1	Stage 2	Stage 3	Stage 4	Stage 5	Stage 6	Stage 7
		↑		↑			
		Event driven		Event driven			

Fig. 10 Planning stage of each model

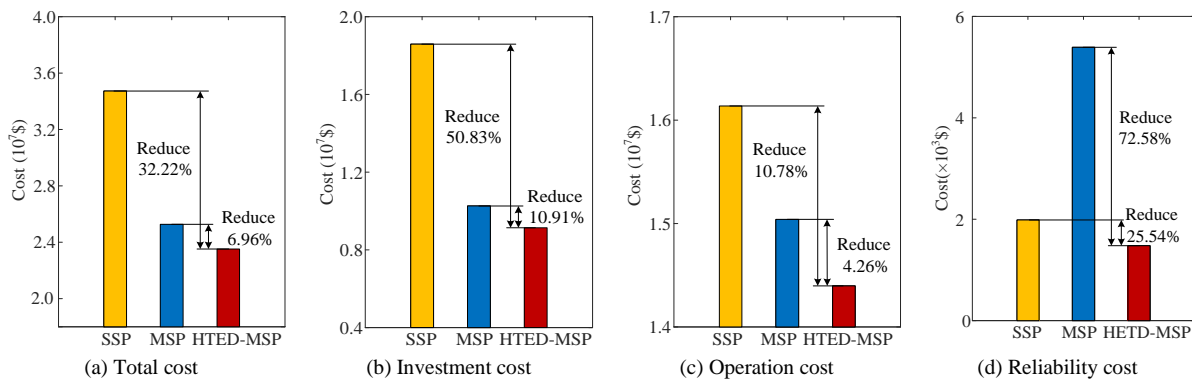
369
370

371 Fig. 10 shows the start time of each planning stage for the SSP, MSP, and HTED-MSP strategies. In the MSP
372 strategy, planning occurs at fixed intervals of every five years. In contrast, the start times in the HTED-MSP strategy
373 are dynamically linked to the forecasting parameters. Unpredictable events in years 10 and 18 trigger event-driven
374 strategies, prompting early transitions to planning stages 3 and 5. However, forecast errors in natural gas prices in
375 years 2 and 3 did not trigger such transitions; a detailed analysis of this is provided in Section 5.3.2.

376 **5.2.1 Planning results of ICES**

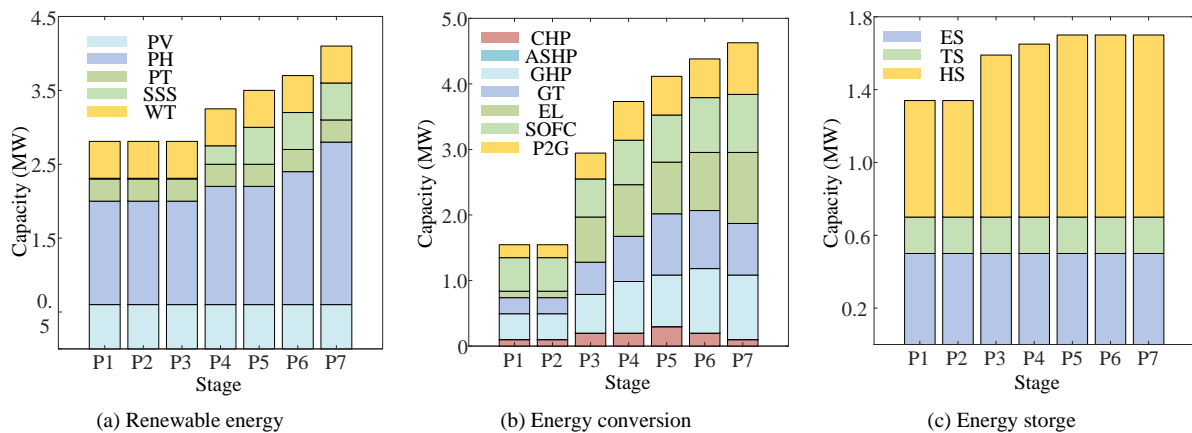
377 Fig. 11 presents the optimal configuration costs for SSP, MSP, and HTED-MSP. The results indicate a
378 progressive decrease in planning costs across the strategies, with the HTED-MSP strategy achieving the most
379 significant reduction, yielding a 50.83% decrease compared to SSP and a 10.91% decrease compared to MSP. The
380 SSP and MSP pre-configure a higher number of redundant devices, which lack long-term competitiveness and
381 consequently lead to increased operational costs. As a result, operational costs under HTED-MSP are reduced by

382 10.78% and 4.26% compared to SSP and MSP, respectively. Notably, SSP incurs lower reliability costs than MSP,
 383 primarily because its planned redundancy serves as a backup in extreme scenarios. However, HTED-MSP provides
 384 the most cost-effective reliability among the three strategies, owing to its ability to dynamically adjust planning
 385 decisions at each stage. Additionally, Fig. 11 highlights the key economic features of the HTED-MSP: it minimizes
 386 the configuration of redundant equipment to ensure cost-effectiveness during the planning stage, while using event-
 387 driven strategy to maintain energy adequacy under long-term growth. Furthermore, HTED-MSP ensures system
 388 reliability through regular equipment replacement by time-driven strategy.

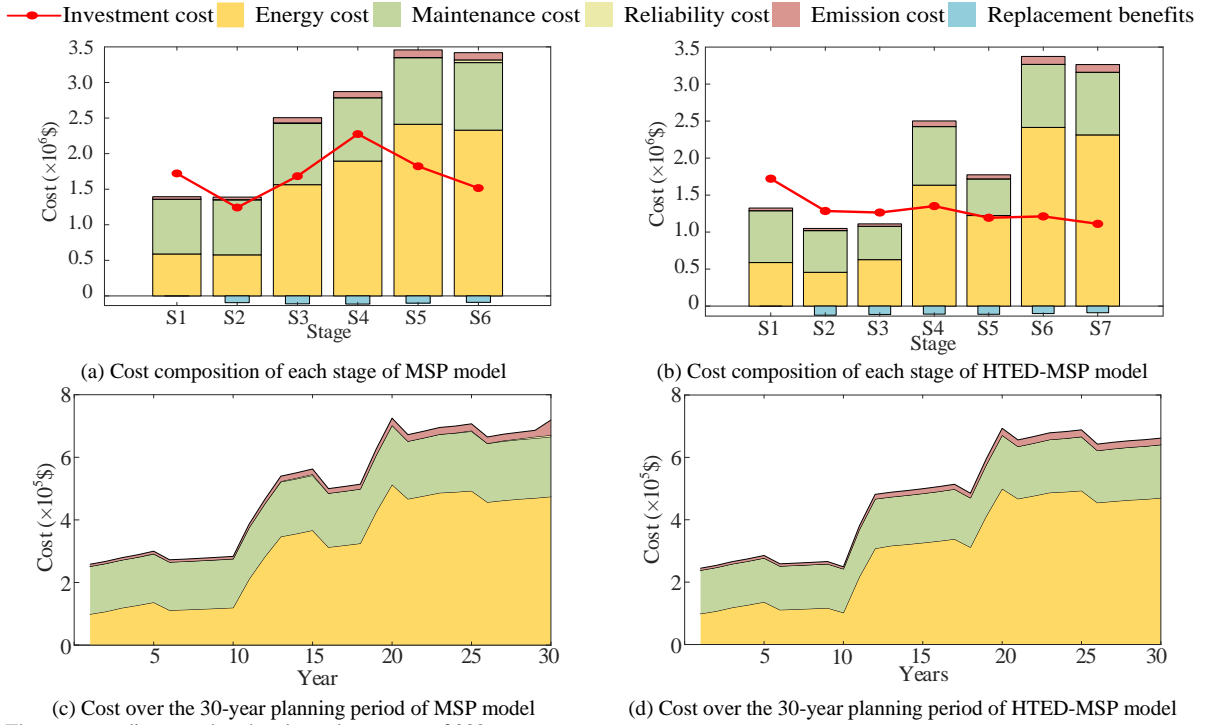


389 **Fig. 11** The planning cost for SSP, MSP, and HTED-MSP

390 Fig. 12 illustrates the installed capacities of various types of equipment. Due to their lower costs, PV and WT
 391 are allocated the maximum capacity. In contrast, the SSS is not implemented in the initial three stages due to its
 392 nascent technology. Additionally, as the costs of hydrogen energy and P2GCC systems decrease, there is a gradual
 393 increase in the deployment of equipment such as EL, SOFC, HS, and P2G, leading to the phasing out of some CHP
 394 and GT units. This shift highlights a trend toward more cost-effective and sustainable energy solutions



395 **Fig. 12** The installed capacities in each stage



* The costs are discounted to the planned start year of 2026.

Fig. 13 The Cost variations during the planning period.

Fig. 13 presents the costs for each stage in the MSP and HTED-MSP planning strategies, along with the annual system operation costs. The equipment replacement benefits reflect the reduction in operating costs due to the replacement of equipment. For both the HTED-MSP and MSP strategies, energy purchase costs are the most significant, comprising approximately 40% to 70% of the total operation costs. Maintenance costs follow, accounting for 20% to 40% of the total operation costs. In comparison, carbon emissions and reliability costs have a relatively smaller impact on the overall costs.

5.2.2 Analysis of the SS method

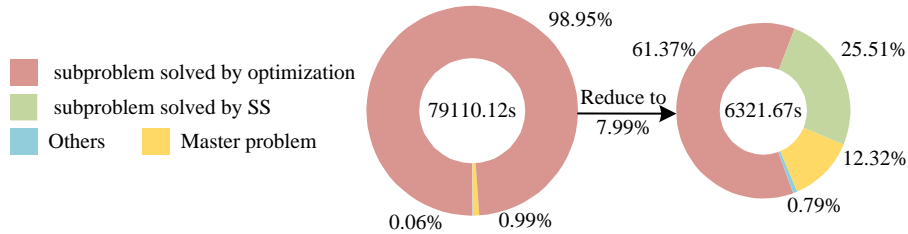
The computational performance of both the BD and SS method are presented in Table 1. First, both methods yield the same planning costs, validating the correctness of the proposed SS method. Meanwhile, the computational time for the SS method is only 7.99% of that for the BD method, owing to the SS method's ability to directly obtain operation decisions for numerous similar scenarios. The "Average number of SS-Sets per year" indicates the limit of efficiency improvement achievable through the SS method. For instance, in the HTED-MSP case, an average of 17.9 SS-Sets implies that only 4.9% (17.9/365) of the scenarios in the SS method need to be optimized. The

411 remaining scenarios can be quickly resolved by solving systems of equations.

412 As shown in Fig. 14, in the BD method, over 98.9% of the time is spent on handling subproblems, with only a
 413 small fraction (0.99%) used for solving the master problem. In contrast, for the SS method, a significant portion of
 414 the optimization process is replaced by equation solving, reducing subproblem processing time to 61.37% of the
 415 total. However, the classification of SS-Sets and the equation-solving process introduce new computational burdens,
 416 approximately accounting for approximately 25.51% of the total computation time.

417 **Table.1** Comparison of planning results using different methods

Method	SSP		MSP		HTED-MSP	
	BD	SS	BD	SS	BD	SS
Total cost ($\times 10^7$ \$)	3.47		2.53		2.35	
Time (s)	184216.25	13871.48	70214.50	5518.86	79110.12	6321.67
Average number of SS-Sets per year	N/A	20.33	N/A	20.21	N/A	17.90



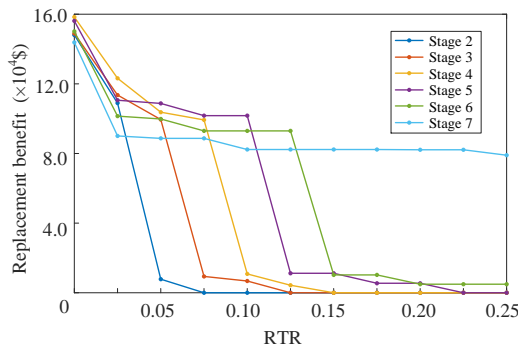
418
 419 *The “Others” refers to the time consumed by operations such as reading data and constructing models.

420 **Fig. 14** Computational time for BD and SS in the HTED-MSP model

421 **5.3. Sensitivity Analysis**

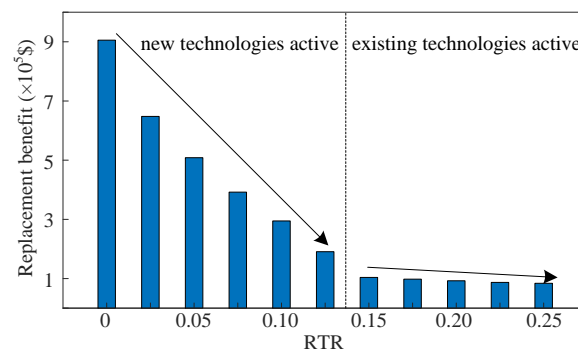
422 This section performs a sensitivity analysis of the RTR and explores why forecast errors in natural gas prices did
 423 not trigger the event-driven strategy from a cost perspective. Additionally, the evolution of low-carbon costs within
 424 the ICES is analyzed.

425 **5.3.1 Sensitivity analysis of RTR**



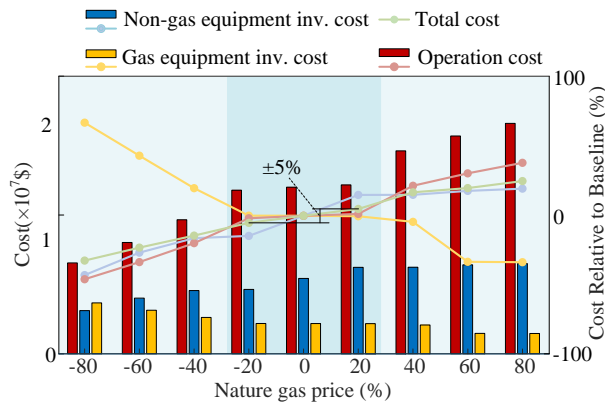
426
 427 **Fig. 15** The impacts of RTR on the replacement benefits for each stage

428 Generally, a higher RTR leads to smaller replacement benefits as shown in Fig. 15, as it restricts the substitution
 429 effect of newer technologies. Interestingly, when RTR is sufficiently low, replacement benefits initially increase
 430 and then decrease over time, indicating that equipment replacement usually occurs in the middle to later stages of
 431 the equipment lifecycle. Moreover, the RTR for the same equipment varies across different stages. For example, in
 432 stage 2, the RTR is approximately 5%, with replacement benefits significantly decreasing when the RTR exceeds
 433 this threshold, whereas in stage 4, the RTR is around 10%. This variation is attributed to technological
 434 advancements that render new technologies more economical over time. Notably, in stage 7, the return rate from
 435 new technologies remains above 25%.



436
 437 **Fig. 16** The relationship between the total system replacement benefits and the RTR

438 As shown in Fig. 16, when the RTR is below 0.125, the replacement benefits exhibit more significant variation.
 439 However, when the RTR exceeds 0.125, the benefits tend to stabilize. This indicates that an RTR higher than 0.125
 440 helps retain existing technological equipment, while an RTR below 0.125 encourages the system to replace older
 441 equipment. Therefore, the RTR plays a critical role in regulating the substitution of old and new technologies. By
 442 adjusting the RTR, planners can strike a balance between promoting technological upgrades and maintaining
 443 system stability and cost-effectiveness, thereby ensuring that the ICES remains competitive and sustainable in an
 444 evolving market and technological environment.



446 **Fig. 17** Impacts of natural gas price fluctuations on costs
447

448 In this section, natural gas prices are allowed to fluctuate within a range of $\pm 80\%$. Changes in equipment
449 investment and operational costs are depicted in Fig. 17. As natural gas prices increase, investment in natural-gas-
450 based equipment decreases significantly, while investment in non-natural-gas equipment rises to meet the energy
451 demands of the ICES. Additionally, within a $\pm 20\%$ fluctuation range of energy prices, the total ICES cost varies
452 by only $\pm 5\%$. However, when energy price fluctuations exceed this threshold, investment costs change dramatically.
453 This indicates that a prediction error of up to 20% in natural gas prices for each planning stage will not significantly
454 impact the planning strategies. Therefore, the 5% forecast errors in natural gas prices in years 2 and 3 did not trigger
455 the event-driven strategy. Similarly, for all long-term uncertainty parameters in ICES, the HTED-MSP model
456 generates sensitivity curves for both single and multiple uncertainty parameters at each planning stage. These
457 sensitivity curves are then used to update the trigger thresholds for the event-driven strategy in the next stage,
458 followed by rolling optimization.

459 Fluctuations in energy prices impact not only the planning costs of ICES but also have a significant influence
460 on carbon emissions. In this section, three scenarios are evaluated: S1, where natural gas prices fluctuate within
461 $\pm 20\%$ of the baseline; S2, where natural gas prices fluctuate within $\pm 80\%$ of the baseline; and S3, where both
462 natural gas and electricity prices fluctuate within $\pm 80\%$ and $\pm 20\%$ of their respective baselines. For each scenario,
463 Monte Carlo simulations are used to assess the impact on carbon emissions. The carbon emission boundaries for
464 these scenarios are depicted in Fig. 18.

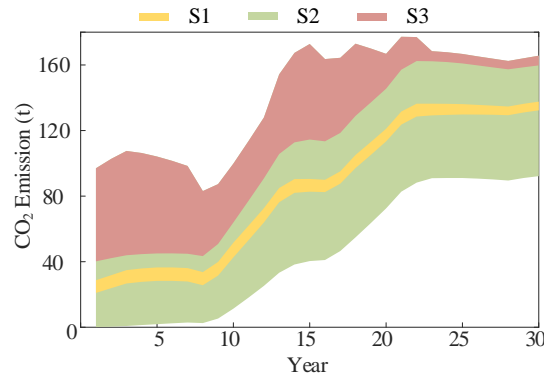


Fig. 18 Impacts of natural gas and electricity price fluctuations on carbon emissions

465
466

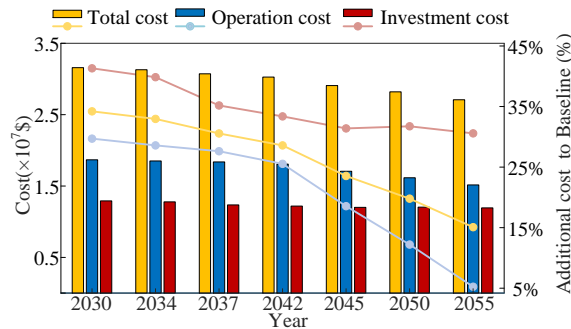
467 Fig. 18 shows that sufficiently high natural gas prices can drive ICES to make planning decisions aimed at lower
 468 carbon targets, even achieving zero carbon emissions in the first 1-3 years of planning. However, as ICES load
 469 demand increases, relying solely on renewable energy becomes insufficient to meet local demands, leading to
 470 higher carbon emissions. Comparing scenarios S2 and S3, a rise in electricity prices is observed not to significantly
 471 affect carbon emissions. In contrast, lower electricity prices have a substantial impact on ICES carbon emissions;
 472 as renewable energy becomes less economically viable compared to cheaper electricity, leading to decreased clean
 473 energy generation.

474 *5.3.3 Cost-time benefit analysis for achieving a zero-carbon ICES*

475 Fig. 19 indicates that achieving zero-carbon ICES planning at the optimal planning point is not feasible,
 476 necessitating additional investment from a cost perspective. The sensitivity analysis results in Fig. 19 show the
 477 timeline for achieving a zero-carbon ICES and the required additional investments. The additional cost rate is
 478 defined as the percentage of extra costs relative to the optimal planning costs. Additionally, it is stipulated that the
 479 ICES can achieve negative carbon emissions by selling electricity to the grid. Generally, emission reduction can be
 480 attained by an increase in the total system cost. For example, to achieve a zero-carbon ICES by 2050, the operational,
 481 investment, and total costs need to increase by 12.2%, 31.7%, and 19.8%, respectively. Furthermore, an accelerated
 482 transition to a zero-carbon ICES leads to higher additional expenses. For instance, reaching this goal by 2030 incurs
 483 14.4% higher additional costs compared to a 2045 target.

484 Upon closer observation, significant differences in sensitivity to economic performance are noted across various
 485 target years for achieving zero carbon. Notably, before 2042, additional investments remain high and are relatively

486 insensitive to time However, after 2042, there is a rapid decrease in additional investments over time, likely due to
 487 factors such as technological advancements and changes in equipment costs. Finally, in all cases, investment costs
 488 are the predominant category of additional costs, accounting for approximately 50% to 78% of the total additional
 489 costs. Operation costs, on the other hand, have a smaller impact on the overall costs.



490
491 **Fig. 19** Impact of zero-carbon target on costs

492 **5.4. Discussion of state similarity**

493 The selection of typical scenarios for analysis has a direct impact on the ICES planning. In particular, for ICES
 494 with high renewable penetration, scenario analysis methods based on a limited number of typical scenarios often
 495 fail to accurately represent real-world operations [34]. In this paper, we directly address massive scenarios without
 496 reduction. Scenarios are classified based on the position of the optimal basis (POB), enabling the rapid and accurate
 497 determination of optimal solutions for massive scenarios. In other words, the SS method has the potential to replace
 498 clustering methods in multi-scenario linear optimization problems. Furthermore, the essence of the SS method lies
 499 in identifying the POB, which means it can be extended to quadratic programming, mixed-integer programming,
 500 and mixed-integer quadratic programming with linear constraints. This will be a focus of our future research.

501 **6. Conclusion**

502 This paper introduces a hybrid time-and-event-driven multi-stage planning (HTED-MSP) model aimed at
 503 mitigating the incremental costs and operational risks caused by unpredictable events or unignorable forecasting
 504 errors. To prevent frequent equipment replacements caused by the dual-driven strategy, a RTR is incorporated, and
 505 its quantitative impact on planning strategies is analyzed. Subsequently, a scenario analysis method based on state
 506 similarity (SS) is developed. By first verifying the positions of the optimal bases (POB) before optimization, this

507 approach significantly accelerates the solution efficiency of large-scale scenario models. Finally, the model is
508 applied to a typical ICES, and the following conclusions are drawn:

- 509 ● The event-driven strategy in the HTED-MSP model dynamically adjusts planning decisions based on
510 unpredictable events or unignorable forecasting errors, it reduces investment costs by 10.91% and
511 operating costs by 4.26% compared to MSP strategy. Moreover, by accounting for operational risks
512 associated with equipment aging during the planning stage, the HTED-MSP model achieves a 72.58%
513 reduction in reliability costs for the ICES.
- 514 ● An appropriate RTR can effectively maintain the vitality of existing technologies The proposed HTED-
515 MSP model offers a pathway for sensitivity analysis to obtain the optimal RTR for a specific community
516 or equipment. Certainly, RTR can also be easily extended to a specific technology, which is highly valuable.
- 517 ● Compared to traditional two-stage methods, the SS method reduces solution time for large-scale scenario-
518 based MILP problems by over 90%. As the number of scenarios increases, the computational efficiency
519 advantages become even more pronounced. Additionally, the SS method can be easily integrated with
520 other acceleration algorithms (such as clustering [49] and IIES [50]) to further enhance computational
521 performance.
- 522 ● According to the future parameter evolution, achieving a zero-carbon ICES is not feasible at the optimal
523 economic planning point. Achieving zero carbon ICES before 2055 would require a 15% cost increase,
524 while aiming for carbon neutrality by 2030 would demand a cost escalation of approximately 34%. These
525 projections underscore the significant financial challenges associated with accelerating the transition to a
526 zero-carbon ICES.

527 Future research will focus on two areas. The first is enhancing the event-driven planning framework by
528 considering factors such as policy changes, for example, examining the impact of low-carbon policies on planning
529 costs. The second area explores the application of state similarity method in nonlinear optimization, particularly in
530 optimal energy flow, enabling their use in regional-scale integrated energy systems analysis.

Nomenclature			
<i>Parameters and Constants</i>			
$A^{PV/PT/PH}$	area of PV / PT / PH	Z^{CHP}	ratio of the change in electrical output power to the thermal output power of the CHP
$R_{t,d,m}^{PV/PT/PH}$	incoming solar radiation per square meter at time t, d, m	η^{CHP}	overall efficiency of CHP
$\eta^{PV/PT/PH}$	energy conversion efficiencies of PV / PT / PH	$\eta^{CHP-CO2}$	carbon emission factor of CHP
q^{H2}	low calorific value of hydrogen	η^{GT-CO2}	carbon emission factor of GT
A^{SSS}	area of SSS	η^{CC}	carbon capture efficiency of CC
$\eta^{SPV/T/H}$	energy conversion efficiency of SSS	η^{C2Q}	carbon capture power consumption factor of CC
$R_{t,d,m}^{SSS}$	incoming solar radiation per square meter at time t, d, m	η^{P2G}	energy conversion efficiency of P2G
$\eta^{dis/ch}$	discharging/charging efficiency of the energy storage	χ	conversion ratio
$\zeta^{max/min}$	max/min limitation energy	$\eta^{SOFC,E}$	electrical conversion efficiency of SOFC
$\eta^{COP,HP}$	COP of HP	$\eta^{SOFC,T}$	thermal energy conversion efficiency of SOFC
q^{gas}	heat value of natural gas	η^{EL}	energy conversion efficiency of EL
η^{GT}	energy conversion efficiency of GT	$L_{t,d,m}^E$	electricity load
η^{g2c}	efficiency of CHP	$L_{t,d,m}^H$	hydrogen load
		$L_{t,d,m}^T$	thermal load
		q^{gas}	heating value of natural gas
<i>Variables*</i>			
$P_{t,d,m}^{PV}$	output electric power of PV at time t, d, m	$P_{t,d,m}^{CHP}$	output power of CHP at time t, d, m
$Q_{t,d,m}^{PT}$	output thermal power of PT at time t, d, m	$Q_{t,d,m}^{CHP}$	output thermal power of CHP at time t, d, m
$H_{t,d,m}^{PH}$	output hydrogen power of PH at time t, d, m	$F_{t,d,m}^{CC}$	carbon capture flow of CC at time t, d, m
$P_{t,d,m}^{SPV}$	output electric power of SSS at time t, d, m	$P_{t,d,m}^{CC}$	carbon capture power of CC at time t, d, m
$Q_{t,d,m}^{SPT}$	output thermal power of SSS at time t, d, m	P^{P2G}	fixed power consumption of the P2GCC system
$H_{t,d,m}^{SPH}$	output hydrogen power of SSS at time t, d, m	$P_{t,d,m}^{P2G}$	power consumption of P2G at time t, d, m
$P_{t,d,m}^{dis/ch}$	discharging/charging power of energy storage at time t, d, m	$F_{t,d,m}^{P2G}$	CH ₄ generated by P2G at time t, d, m
$P_{t,d,m}^{dis,ch,max}$	the max discharging/charging of energy storage at time t, d, m	$H_{t,d,m}^{P2G}$	hydrogen consumption of P2G at time t, d, m
		$P_{t,d,m}^{P2GCC}$	fixed power consumption of the P2GCC system at time t, d, m
$P_{t,d,m}^{HP}$	input electric power of HP at time t, d, m	$H_{t,d,m}^{SOFC}$	input hydrogen power of SOFC at time t, d, m
$Q_{t,d,m}^{HP}$	output thermal power of HP at time t, d, m	$P_{t,d,m}^{SOFC}$	output electric power of SOFC at time t, d, m
$F_{t,d,m}^{GT}$	input gas flow of GT at time t, d, m	$Q_{t,d,m}^{SOFC}$	output thermal power of SOFC at time t, d, m
$P_{t,d,m}^{GT}$	output power of GT at time t, d, m	$H_{t,d,m}^{EL}$	output hydrogen power of EL at time t, d, m
$F_{t,d,m}^{CHP}$	fuel input power of CHP	$P_{t,d,m}^{EL}$	input electric power of EL at time t, d, m
$F_{t,d,m}^{CHP}$	fuel consumption flow of CHP at time t, d, m	$R_{t,d,m}^E$	load shedding of electricity
$P_{t,d,m}^{CON}$	power of the extraction condensing CHP unit in full condensing mode	$R_{t,d,m}^H$	load shedding of hydrogen energy
		$R_{t,d,m}^T$	load shedding of thermal energy

* The domain of all variables in this table is $\mathbb{R}_{\geq 0} = \{x \in \mathbb{R} | x \geq 0\}$.

533 A.1 Solar supply unit model

534 PV, PT, and PH systems can convert solar energy into electrical, thermal, and hydrogen energy, respectively. The associated constraints can
535 be formalized as follows:

536
$$P_{t,d,m}^{PV} = \eta^{PV} A^{PV} R_{t,d,m}^{PV} \tag{A1}$$

537
$$Q_{t,d,m}^{PT} = \eta^{PT} A^{PT} R_{t,d,m}^{PT} \tag{A2}$$

538
$$H_{t,d,m}^{PH} = \eta^{PH} A^{PH} R_{t,d,m}^{PH} / q^{H_2} \tag{A3}$$

539 To enhance energy conversion efficiency, an integrated solar energy system is proposed in [27][28]. The system integrates PV, PH, and PT
540 technologies, and employs a specialized dielectric layer to partition sunlight into three distinct spectral bands. i) The spectral range between 500
541 nm and 800 nm is utilized for PV generation. ii) The spectral band with wavelengths greater than 800 nm is harnessed for solar thermal collection.
542 iii) The spectral band with wavelengths shorter than 500nm is employed for photocatalytic hydrogen production. The constraints for the solar
543 spectral splitting unit can be expressed as follows:
544

545
$$P_{t,d,m}^{SPV} = \eta^{SPV} A^{SSS} R_{t,d,m}^{SSS} \tag{A4}$$

546
$$Q_{t,d,m}^{SPT} = \eta^{SPT} A^{SSS} R_{t,d,m}^{SSS} \tag{A5}$$

547
$$H_{t,d,m}^{SPH} = \eta^{SPH} A^{SSS} R_{t,d,m}^{SSS} / q^{H_2} \tag{A6}$$

548 A.2 Energy storage model

549 The operation constraints for energy storage are as follows:

$$550 \quad 0 \leq P_{t,d,m}^{\text{ch}} \leq U_{t,d,m}^{\text{ch}} P^{\text{ch,max}} \quad (\text{A7})$$

$$551 \quad 0 \leq P_{t,d,m}^{\text{dis}} \leq U_{t,d,m}^{\text{dis}} P^{\text{dis,max}} \quad (\text{A8})$$

$$552 \quad U_{t,d,m}^{\text{dis}} \cdot U_{t,d,m}^{\text{ch}} = 0 \quad (\text{A9})$$

$$553 \quad S_{t=0,d,m} = S_{t=0,d+1,m} \quad (\text{A10})$$

$$554 \quad S_{t,d,m} = S_{t-1,d,m} + \eta^{\text{ch}} P_{t,d,m}^{\text{ch}} - P_{t,d,m}^{\text{dis}} / \eta^{\text{dis}} \quad (\text{A11})$$

$$555 \quad S^{\text{min}} \leq S_{t,d,m} \leq S^{\text{max}} \quad (\text{A12})$$

556 where $U_{t,d,m}^{\text{dis/ch}} \in \{ U_{t,d,m}^{\text{dis/ch}} \in \mathbb{N} \mid 0 \leq U_{t,d,m}^{\text{dis/ch}} \leq 1 \}$ is the discharging/charging factor of energy storage at time t, d, m . $S_{t,d,m} \in \mathbb{R}_{\geq 0}$ donates the capacity of
557 energy storage at time t, d, m . However, (A9) leads to the non-convexity of the model. [51] has demonstrated that relaxing this constraint does
558 not affect the variation of the objective function. This is because the energy loss caused by charging and discharging further reduces the system's
559 economic efficiency.

560 A.3 Energy conversion equipment model

$$561 \quad Q_{t,d,m}^{\text{HP}} = \eta^{\text{COP,HP}} P_{t,d,m}^{\text{HP}} \quad (\text{A13})$$

$$562 \quad P_{t,d,m}^{\text{GT}} = \eta^{\text{GT}} q^{\text{gas}} F_{t,d,m}^{\text{GT}} \quad (\text{A14})$$

563 A.4 CHP model

565 In this section, the extraction condensing steam turbine CHP unit is chosen for modeling. The energy conversion model is described in (A15)
566 - (A17)

$$567 \quad P_{\text{CON}}^{\text{CHP}} = \eta^{\text{g2e}} F^{\text{CHP}} \quad (\text{A15})$$

$$568 \quad P_{t,d,m}^{\text{CHP}} = -Q_{t,d,m}^{\text{CHP}} / Z^{\text{CHP}} + P_{\text{CON}}^{\text{CHP}} \quad (\text{A16})$$

$$569 \quad q^{\text{gas}} \eta^{\text{CHP}} F_{t,d,m}^{\text{CHP}} = Q_{t,d,m}^{\text{CHP}} + P_{t,d,m}^{\text{CHP}} \quad (\text{A17})$$

570 A.5 P2GCC Model

571 The CP primarily utilizes carbon capture devices to capture the carbon dioxide emitted by CHP and GT units and integrate carbon storage.
572 The captured carbon dioxide is processed through the P2G system to produce methane, which is directly supplied to the GT and CHP to realize
573 the recycling of CO2. The P2G-CC model can be formulated as follows:

$$574 \quad F_{t,d,m}^{\text{CC}} = \eta^{\text{CC}} (\eta^{\text{GT-CO}_2} P_{t,d,m}^{\text{GT}} + \eta^{\text{CHP-CO}_2} Q_{t,d,m}^{\text{CHP}}) \quad (\text{A18})$$

$$575 \quad P_{t,d,m}^{\text{CC}} = \eta^{\text{C2Q}} F_{t,d,m}^{\text{CC}} \quad (\text{A19})$$

$$576 \quad P_{t,d,m}^{\text{P2GCC}} = P_{t,d,m}^{\text{P2G}} + P_{t,d,m}^{\text{CC}} + P^{\text{ga}} \quad (\text{A20})$$

$$577 \quad F_{t,d,m}^{\text{P2G}} = \eta^{\text{P2G}} P_{t,d,m}^{\text{P2G}} / q^{\text{gas}} \quad (\text{A21})$$

$$578 \quad P_{t,d,m}^{\text{P2G}} = \chi H_{t,d,m}^{\text{P2G}} \quad (\text{A22})$$

579 A.6 SOFC model

580 The operational characteristics of the SOFC can be described as follows:

$$581 \quad P_{t,d,m}^{\text{SOFC}} = \eta^{\text{SOFC,E}} H_{t,d,m}^{\text{SOFC}} \quad (\text{A23})$$

$$582 \quad Q_{t,d,m}^{\text{SOFC}} = \eta^{\text{SOFC,T}} H_{t,d,m}^{\text{SOFC}} \quad (\text{A24})$$

583 A.7 EL model

584 The operational model of EL can be described as follows:

$$585 \quad H_{t,d,m}^{\text{EL}} = \eta^{\text{EL}} P_{t,d,m}^{\text{EL}} / q^{\text{H}_2} \quad (\text{A25})$$

586 A.8 Energy flow model

587 In summary, the energy flow equations for electricity, heating, hydrogen, and natural gas can be formulated as follows,

588
$$P_{t,d,m}^{grid} + P_{t,d,m}^{PV} + P_{t,d,m}^{SPV} - P_{t,d,m}^{ES, ch} + P_{t,d,m}^{ES, dis} + P_{t,d,m}^{GT} + P_{t,d,m}^{CHP} + P_{t,d,m}^{P2GCC} + P_{t,d,m}^{SOFC} - P_{t,d,m}^{HP} - P_{t,d,m}^{EL} = L_{t,d,m}^E - R_{t,d,m}^E \quad (A26)$$

589
$$Q_{t,d,m}^{PT} + Q_{t,d,m}^{SPT} - Q_{t,d,m}^{TS, ch} + Q_{t,d,m}^{TS, dis} + Q_{t,d,m}^{HP} + Q_{t,d,m}^{CHP} + Q_{t,d,m}^{SOFC} = L_{t,d,m}^T - R_{t,d,m}^T \quad (A27)$$

590
$$H_{t,d,m}^{PH} + H_{t,d,m}^{SPH} - H_{t,d,m}^{HS, ch} + H_{t,d,m}^{HS, ch} - H_{t,d,m}^{P2G} - H_{t,d,m}^{SOFC} + H_{t,d,m}^{EL} = L_{t,d,m}^H - R_{t,d,m}^H \quad (A28)$$

591
$$F_{t,d,m}^{gas} + F_{t,d,m}^{P2G} - F_{t,d,m}^{GT} - F_{t,d,m}^{CHP} = 0 \quad (A29)$$

592 **Appendix B. Parameters of ICES Equipment**

593 Tables B.1 to B.3 present the dynamic costs and technical parameters of the devices within the ICES system. The specific parameters for
 594 SOFC, CC+GT, PV, PT, CHP, GHP, ASHP, WT, and ES are sourced from references [8], [40], and [41]. However, there is a lack of predictive
 595 parameters for devices PH, TS, HS, and SSS in existing research. Therefore, based on the current economic and technical parameters from
 596 references [27], we have constructed future parameters for PH, TS, HS, and SSS.

597 **Table B.1**
 598 Cost and technical parameters of the SOFC, CP, GT, PV, PH, and EL.

Year	SOFC [40]			GT+CC [41]		PV [27] [41]		PH [27] [41]		EL [41]	
	C ^{inv} (\$/kW)	Eff _{elc}	Eff _{th}	C ^{inv} (\$/kW)	Eff	C ^{inv} (\$/m ²)	Eff	C ^{inv} (\$/m ²)	Eff	C ^{inv} (\$/kW)	Eff
1	6238	0.560	0.610	2001	0.500	96	0.200	131	0.100	2300	0.700
2	6228	0.561	0.611	1999	0.502	94	0.201	129	0.102	2269	0.703
3	6218	0.562	0.612	1996	0.504	91	0.202	127	0.103	2239	0.707
4	6208	0.563	0.613	1994	0.506	88	0.203	124	0.105	2208	0.710
5	6198	0.564	0.614	1992	0.508	86	0.204	122	0.107	2177	0.713
6	6188	0.565	0.615	1990	0.510	83	0.205	120	0.108	2147	0.717
7	6177	0.566	0.616	1987	0.512	80	0.206	118	0.110	2116	0.720
8	6167	0.567	0.617	1985	0.514	77	0.207	116	0.112	2085	0.723
9	6157	0.568	0.618	1983	0.516	75	0.208	114	0.113	2055	0.727
10	6147	0.569	0.619	1980	0.518	72	0.209	111	0.115	2024	0.730
11	6137	0.570	0.620	1978	0.520	69	0.210	109	0.117	1993	0.733
12	6124	0.572	0.622	1970	0.522	68	0.211	107	0.118	1963	0.737
13	6111	0.574	0.624	1962	0.524	66	0.212	105	0.118	1932	0.740
14	6099	0.576	0.626	1954	0.526	65	0.213	103	0.119	1901	0.743
15	6086	0.578	0.628	1946	0.528	64	0.214	100	0.120	1871	0.747
16	6073	0.580	0.630	1938	0.530	62	0.215	98	0.121	1840	0.750
17	6060	0.582	0.632	1930	0.532	61	0.216	96	0.122	1791	0.750
18	6047	0.584	0.634	1922	0.534	59	0.217	94	0.123	1740	0.750
19	6035	0.586	0.636	1914	0.536	58	0.218	92	0.123	1691	0.750
20	6022	0.588	0.638	1906	0.538	56	0.219	90	0.124	1641	0.750
21	6009	0.590	0.640	1898	0.540	55	0.220	87	0.125	1590	0.750
22	5999	0.591	0.641	1898	0.541	54	0.221	84	0.125	1541	0.750
23	5989	0.592	0.642	1898	0.542	53	0.222	80	0.125	1492	0.750
24	5979	0.593	0.643	1898	0.543	52	0.223	77	0.125	1441	0.750
25	5969	0.594	0.644	1898	0.544	51	0.224	73	0.125	1392	0.750
26	5959	0.595	0.645	1898	0.545	50	0.225	70	0.125	1342	0.750
27	5948	0.596	0.646	1898	0.546	50	0.226	66	0.125	1291	0.750
28	5938	0.597	0.647	1898	0.547	49	0.227	62	0.125	1242	0.750
29	5928	0.598	0.648	1898	0.548	48	0.228	59	0.125	1193	0.750
30	5908	0.600	0.650	1898	0.550	46	0.230	52	0.125	1093	0.750

599 **Table B.2**
 600 Cost and technical parameters of the CHP+CC, GHP, ASHP, WT, ES, and P2G. It is noteworthy that CHP, GHP, and ASHP, besides having
 601 dynamic costs (\$/kW), also possess fixed installation costs (\$). For detailed data, please refer to [8].

Year	CHP+CC [8]	GHP [8]	ASHP [8]	WT [41]	ES [8]	P2G [41]
------	------------	---------	----------	---------	--------	----------

	C^{inv} (\$/kW)	Eff_elc	Eff_th	C^{inv} (\$/kW)	Eff	C^{inv} (\$/kW)	Eff	C^{inv} (\$/kW)	Eff	C^{inv} (\$/ kWh)	C^{inv} (\$/kW)	Eff
1	909	0.300	0.550	2818	4.00	702	3.00	2875	0.400	276	1725	0.700
2	904	0.301	0.551	2721	4.02	683	3.00	2842	0.400	270	1696	0.705
3	899	0.302	0.552	2627	4.04	665	3.03	2809	0.400	266	1668	0.710
4	895	0.303	0.553	2537	4.08	647	3.06	2776	0.400	261	1639	0.715
5	890	0.304	0.554	2450	4.12	630	3.09	2744	0.400	255	1610	0.720
6	886	0.305	0.555	2366	4.17	613	3.12	2711	0.400	251	1581	0.725
7	882	0.306	0.556	2284	4.21	597	3.16	2677	0.400	246	1553	0.730
8	877	0.307	0.557	2206	4.25	581	3.19	2645	0.400	242	1524	0.735
9	873	0.308	0.558	2130	4.29	565	3.22	2612	0.400	240	1495	0.740
10	868	0.309	0.559	2056	4.33	550	3.25	2579	0.400	232	1466	0.745
11	864	0.310	0.560	2019	4.37	536	3.28	2546	0.400	228	1438	0.750
12	860	0.312	0.562	1917	4.41	521	3.31	2529	0.400	224	1409	0.760
13	856	0.314	0.564	1852	4.46	507	3.34	2512	0.400	220	1380	0.770
14	851	0.316	0.566	1787	4.50	493	3.37	2493	0.400	216	1351	0.780
15	848	0.318	0.568	1726	4.54	481	3.40	2476	0.400	212	1323	0.790
16	843	0.320	0.570	1666	4.58	468	3.43	2459	0.400	208	1294	0.800
17	838	0.322	0.572	1609	4.62	455	3.47	2441	0.400	204	1265	0.810
18	835	0.324	0.574	1554	4.66	443	3.50	2424	0.400	200	1236	0.820
19	830	0.326	0.576	1501	4.70	431	3.53	2406	0.400	197	1208	0.830
20	826	0.328	0.578	1449	4.74	420	3.56	2389	0.400	192	1179	0.840
21	822	0.330	0.580	1400	4.79	408	3.59	2371	0.400	189	1150	0.850
22	818	0.333	0.582	1351	4.83	398	3.62	2341	0.401	185	1127	0.853
23	814	0.336	0.584	1304	4.87	388	3.65	2312	0.402	182	1104	0.856
24	810	0.339	0.586	1236	4.91	377	3.68	2280	0.403	178	1081	0.859
25	806	0.342	0.588	1217	4.95	367	3.71	2251	0.404	175	1058	0.862
26	802	0.345	0.590	1174	4.99	358	3.74	2221	0.405	171	1035	0.865
27	798	0.348	0.592	1134	5.03	347	3.78	2191	0.406	169	1012	0.868
28	794	0.351	0.594	1095	5.08	338	3.81	2161	0.407	166	989	0.871
29	790	0.354	0.596	1058	5.12	329	3.84	2130	0.408	162	966	0.874
30	785	0.360	0.600	1021	5.20	321	3.90	2070	0.410	156	920	0.880

602
603

Table B.3
The initial cost and technical parameters of the PT, TS, and HS.

Parameter	PT [27]	TS [27]	HS [27]
C^{inv}	76 (\$/m ²)	32.9 (\$/kWh)	571 (\$/kg)
Eff (%)	0.472	0.90	0.95

604
605

Table B.4
The initial cost and technical parameters of SSS[27].

Parameter	SSS
C^{inv} (\$/m ²)	304
Proportion of solar radiation loss (%)	11.8
Proportion of solar radiation for PV (%)	24
Proportion of solar radiation for PT (%)	48
Proportion of solar radiation for PH (%)	16.2
PV-efficiency (%)	41.5
PT-efficiency (%)	41.9
PH-efficiency (%)	47.2

606
607

Table B.5
Cost parameters of PT, TS, HS, and SSS.

Year	PT	TS	HS	SSS
	C^{inv} (\$/m ²)	C^{inv} (\$/kWh)	C^{inv} (\$/kg)	C^{inv} (\$/m ²)
1	76	32.9	571	304
2	75	32.8	564	299
3	74	32.8	556	296
4	73	32.7	549	291
5	72	32.7	541	287
6	71	32.7	533	283
7	70	32.6	526	279
8	69	32.6	518	275
9	68	32.5	511	271

10	67	32.5	503	267
11	66	32.5	495	263
12	65	32.4	488	259
13	64	32.4	480	255
14	63	32.4	472	251
15	62	32.3	465	247
16	61	32.3	457	243
17	59	32.3	445	236
18	58	32.2	432	230
19	56	32.2	420	223
20	55	32.2	408	217
21	53	32.1	395	210
22	51	32.1	383	203
23	50	32.1	371	197
24	48	32.0	358	190
25	46	32.0	346	184
26	45	32.0	333	177
27	43	32.0	321	170
28	41	32.0	309	164
29	40	32.0	296	157
30	36	31.9	271	144

608 **Table B.6**
609 Lifetime, yearly conversion degradation coefficient, reliability index, and maintenance cost, and capacity of all energy conversion and
610 generation equipment[8], [27], [40], [41], [42], [43], [44], [47].

Parameter	CC+GT	PV	PT	PH	CHP+CC	GHP	ASHP	WT	SSS	P2G	SOFC	EL
Lifetime (years)	20	25	20	20	30	20	20	25	15	20	10	20
Yearly conversion degradation coefficient (%)	1	0.5	1	1	2	2	2	1	2	2	2	2
Reliability decay factor μ	6	5	4	5	6	6	6	4	4	6	6	6
Maintenance cost (\$/kWh)	0.44	0	0.01	0.1	0.99	0.01	0.01	0.093	10	0.27	0	0.2

611 **Table B.7**
612 Technical parameters of ES, TS, and HS[8], [46], [45], [48].

Parameter	ES	TS	HS
Lifetime (years)	15	30	20
Charge/discharge efficiency (%)	90	90	95
Maximum charge/discharge rate (%)	20	20	20
Self-discharge rate (%)	0.06	0.5	0.1
Upper bound of SOC	0.9	0.9	0.9
Lower bound of SOC	0.1	0.1	0.1
Degradation parameters	Table B.8	Table B.9	-
Reliability decay factor μ	4	6.5	5
Maintenance cost (\$/kW)	0.01	0	0.01

613 **Table B.8**
614 Degradation parameters of ES [29].

Parameter	Value
α ($\text{kW}^{-1} \text{K}^{-2}$)	5.04e^{-6}
β ($\text{kW}^{-1} \text{K}^{-1}$)	-2.998e^{-3}
γ (kW^{-1})	0.446
δ ($\text{K}^{-1} \text{h}$)	-3.35e^{-3}
ε (h)	1.175
θ	4944
Ea (J mol^{-1})	24 500
R ($\text{J mol}^{-1} \text{K}^{-1}$)	8.314
K (K)	288

615 **Table B.9**
616 Degradation parameters of TS [29].

Parameter	Value
ζ^{TS} (%)	0
θ^{storage} (%) [31]	0.060
θ^{static} (%) [31]	0.053

617 **Reference**

- 618 [1] Shen Y, Kwan T H, Yang H. Parametric and global seasonal analysis of a hybrid PV/T-CCA system for combined CO₂ capture and
619 power generation. *Applied Energy*, 2022, 311: 118681.
- 620 [2] Chen Y, Pei W, Xiao H, et al. Incentive-compatible and budget balanced AGV mechanism for peer-to-peer energy trading in smart grids.
621 *Global Energy Interconnection*, 2023, 6(1): 26-35.
- 622 [3] Yu K, van Son P. Review of trans-Mediterranean power grid interconnection: A regional roadmap towards energy sector decarbonization.
623 *Global Energy Interconnection*, 2023, 6(1): 115-126.
- 624 [4] Mehedi H, Wang X, Ye S, et al. Power generation expansion planning approach considering carbon emission constraints. *Global Energy*
625 *Interconnection*, 2023, 6(2): 127-140.
- 626 [5] Podkovalnikov S, Chudinova L, Trofimov I L, et al. Caspian energy ring: Prospective vision. *Global Energy Interconnection*, 2022, 5(5):
627 461-471.
- 628 [6] National Renewable Energy Laboratory. Annual Technology Baseline. 2020, URL <https://atb.nrel.gov/archive>.
- 629 [7] International Energy Agency. Renewables 2023: Analysis and forecasts to 2028, URL https://iea.blob.core.windows.net/assets/3f7f2c25-5b6f-4f3c-a1c0-71085bac5383/Renewables_2023.pdf
- 630 [8] Mavromatidis G, Petkov I. MANGO: A novel optimization model for the long-term, multi-stage planning of decentralized multi-energy
631 systems. *Applied Energy*, 2021, 288: 116585.
- 632 [9] Lei Y, Wang D, Jia H, et al. Multi-stage stochastic planning of regional integrated energy system based on scenario tree path optimization
633 under long-term multiple uncertainties. *Applied Energy*, 2021, 300: 117224.
- 634 [10] Li J, Zhang L, Zhang B, et al. Coordinated planning for flexible interconnection and energy storage system in low-voltage distribution
635 networks to improve the accommodation capacity of photovoltaic. *Global Energy Interconnection*, 2023, 6(6): 700-713.
- 636 [11] Li H, Liu W. Coordinated Cyber-Physical equipment planning for distributed generation based on chance constrained. *Global Energy*
637 *Interconnection*, 2022, 5(6): 645-653.
- 638 [12] Davoudkhani I F, Dejamkhooy A, Nowdeh S A. A novel cloud-based framework for optimal design of stand-alone hybrid renewable
639 energy system considering uncertainty and battery aging. *Applied Energy*, 2023, 344: 121257.
- 640 [13] Eshraghi H, de Queiroz A R, DeCarolis J F. US energy-related greenhouse gas emissions in the absence of federal climate policy.
641 *Environmental science & technology*, 2018, 52(17): 9595-9604.
- 642 [14] Cano E L, Groissböck M, Moguerza J M, et al. A strategic optimization model for energy systems planning. *Energy and buildings*, 2014,
643 81: 416-423.
- 644 [15] Pecena Z K, Stadler M, Fahy K. Efficient multi-year economic energy planning in microgrids. *Applied Energy*, 2019, 255: 113771.
- 645 [16] Wei J, Zhang Y, Wang J, et al. Multi-period planning of multi-energy microgrid with multi-type uncertainties using chance constrained
646 information gap decision method. *Applied Energy*, 2020, 260: 114188.
- 647 [17] Faraji J, Hashemi-Dezaki H, Ketabi A. Multi-year load growth-based optimal planning of grid-connected microgrid considering long-
648 term load demand forecasting: A case study of Tehran, Iran. *Sustainable Energy Technologies and Assessments*, 2020, 42: 100827.
- 649 [18] HOMER. HOMER Pro - Microgrid Software for Designing Optimized Hybrid Microgrids. HOMER Energy LLC; 2020, URL
650 <https://www.homerenergy.com/products/pro/index.html>.
- 651 [19] Lei D, Zhang Z, Wang Z, et al. Long-term, multi-stage low-carbon planning model of electricity-gas-heat integrated energy system
652 considering ladder-type carbon trading mechanism and CCS. *Energy*, 2023: 128113.
- 653 [20] Khazaeni Y, Cassandras C G. Event excitation for event-driven control and optimization of multi-agent systems. 13th International
654 Workshop on Discrete Event Systems (WODES). IEEE, 2016: 197-202.
- 655

- 656 [21] Maschio D M R, Duarte B, Lazzaretti A E, et al. An event-driven approach for resources planning in distributed power generation
657 systems. *International Journal of Electrical Power & Energy Systems*, 2022, 137: 107768.
- 658 [22] Li P, Li S, Yu H, et al. Quantized event-driven simulation for integrated energy systems with hybrid continuous-discrete dynamics.
659 *Applied Energy*, 2022, 307: 118268.
- 660 [23] Papaemmanouil A, Tjernberg L B, Tuan L A, et al. Improved cost-benefit analysis for market-based transmission planning, a European
661 perspective. *Energy policy*, 2013, 63: 215-223.
- 662 [24] Song G, Lin M, Yu H, et al. Reliability-constrained planning of community integrated energy systems based on fault incidence matrix.
663 *International Journal of Electrical Power & Energy Systems*, 2024, 155: 109559.
- 664 [25] Yang B, Ge S, Liu H, et al. Regional integrated energy system reliability and low carbon joint planning considering multiple uncertainties.
665 *Sustainable Energy, Grids and Networks*, 2023, 35: 101123.
- 666 [26] Yang B, Huang X, Wang S, et al. An Economy and Reliability Co-optimization Planning Method for Regional Integrated Energy Systems.
667 2022 IEEE 6th Conference on Energy Internet and Energy System Integration (EI2). IEEE, 2022: 933-939.
- 668 [27] Chen Z, Yiliang X, Hongxia Z, et al. Optimal design and performance assessment for a solar powered electricity, heating and hydrogen
669 integrated energy system. *Energy*, 2023, 262: 125453.
- 670 [28] Pinaud B A, Benck J D, Seitz L C, et al. Technical and economic feasibility of centralized facilities for solar hydrogen production via
671 photocatalysis and photoelectrochemistry. *Energy & Environmental Science*, 2013, 6(7): 1983-2002.
- 672 [29] Cardoso G, Brouhard T, DeForest N, et al. Battery aging in multi-energy microgrid design using mixed integer linear programming.
673 *Applied energy*, 2018, 231: 1059-1069.
- 674 [30] Alabi T M, Lu L, Yang Z. A novel multi-objective stochastic risk co-optimization model of a zero-carbon multi-energy system (ZCMES)
675 incorporating energy storage aging model and integrated demand response. *Energy*, 2021, 226: 120258.
- 676 [31] Steen D, Stadler M, Cardoso G, et al. Modeling of thermal storage systems in MILP distributed energy resource models. *Applied Energy*,
677 2015, 137: 782-792.
- 678 [32] Zeng Z, Ding T, Xu Y, et al. Reliability evaluation for integrated power-gas systems with power-to-gas and gas storages. *IEEE*
679 *Transactions on Power Systems*, 2019, 35(1): 571-583.
- 680 [33] Liu Z, Tang P, Hou K, et al. A Lagrange-multiplier-based Reliability Assessment for Power Systems Considering Topology and Injection
681 Uncertainties. *IEEE Transactions on Power Systems*, 2023.
- 682 [34] Liu Z, Hou K, Jia H, et al. A Lagrange multiplier based state enumeration reliability assessment for power systems with multiple types
683 of loads and renewable generations. *IEEE Transactions on Power Systems*, 2020, 36(4): 3260-3270.
- 684 [35] Bradley J V. The insidious L-shaped distribution. *Bulletin of the Psychonomic Society*, 1982, 20(2): 85-88.
- 685 [36] Birge J R, Louveaux F. Introduction to stochastic programming. Springer Science & Business Media, 2011.
- 686 [37] Pistikopoulos E N, Diangelakis N A, Oberdieck R. Multi-parametric optimization and control. John Wiley & Sons, 2020.
- 687 [38] Dantzig G B. Origins of the simplex method. *A history of scientific computing*. 1990: 141-151.
- 688 [39] ANALYSIS & PROJECTIONS. Energy Information Administration; 2023, URL [https://www.eia.gov/analysis/projection-](https://www.eia.gov/analysis/projection-data.php#annualproj)
689 [data.php#annualproj](https://www.eia.gov/analysis/projection-data.php#annualproj)
- 690 [40] Annual Energy Outlook 2023. Energy Information Administration; 2023, URL <https://www.eia.gov/outlooks/aeo/>
- 691 [41] SCCER JASM. Energy conversion technologies in STEM. 2020, Available from: [https://data.sccer-
692 jasm.ch/energy-conversion-
693 technologies-stem/2020-03-05/](https://data.sccer-jasm.ch/energy-conversion-technologies-stem/2020-03-05/).
- 693 [42] Pu Y, Li Q, Zou X, et al. Optimal sizing for an integrated energy system considering degradation and seasonal hydrogen storage. *Applied*
694 *Energy*, 2021, 302: 117542.
- 695 [43] Jiang Q, Mu Y, Jia H, et al. A Stackelberg Game-based planning approach for integrated community energy system considering multiple
696 participants. *Energy*, 2022, 258: 124802.
- 697 [44] Mu Y, Chen W, Yu X, et al. A double-layer planning method for integrated community energy systems with varying energy conversion
698 efficiencies. *Applied Energy*, 2020, 279: 115700.

- 699 [45] Pan G, Gu W, Lu Y, et al. Optimal planning for electricity-hydrogen integrated energy system considering power to hydrogen and heat
700 and seasonal storage. *IEEE Transactions on Sustainable Energy*, 2020, 11(4): 2662-2676.
- 701 [46] Zamfirescu C, Dincer I. Assessment of a new integrated solar energy system for hydrogen production. *Solar Energy*, 2014, 107: 700-
702 713.
- 703 [47] Jordan D C, Kurtz S R. Photovoltaic degradation rates—an analytical review. *Progress in photovoltaics: Research and Applications*,
704 2013, 21(1): 12-29.
- 705 [48] Stadler M, Groissböck M, Cardoso G, et al. Optimizing Distributed Energy Resources and building retrofits with the strategic DER-
706 CAModel. *Applied Energy*, 2014, 132: 557-567.
- 707 [49] Milligan G W, Cooper M C. Methodology review: Clustering methods. *Applied psychological measurement*, 1987, 11(4): 329-354.
- 708 [50] Hou K, Jia H, Li X, et al. Impact - increment based decoupled reliability assessment approach for composite generation and transmission
709 systems. *IET Generation, Transmission & Distribution*, 2018, 12(3): 586-595.
- 710 [51] Li Z, Guo Q, Sun H, et al. Storage-like devices in load leveling: Complementarity constraints and a new and exact relaxation method.
711 *Applied Energy*, 2015, 151: 13-22.